



Full length article

Is biomass burning always a dominant contributor of fine aerosols in upper northern Thailand?

Wenhui Song^{a,b,c}, Yan-Lin Zhang^{a,b,*}, Yuxian Zhang^{a,b}, Fang Cao^{a,b}, Martin Rauber^c, Gary Salazar^c, Sawaeng Kawichai^d, Tippawan Prapamontol^d, Sönke Szidat^c

^a School of Applied Meteorology, Nanjing University of Information Science & Technology, Nanjing 210044, China

^b Atmospheric Environment Center, Joint Laboratory for International Cooperation on Climate and Environmental Change, Ministry of Education (ILCEC), Nanjing University of Information Science & Technology, Nanjing 210044, China

^c Department of Chemistry, Biochemistry and Pharmaceutical Sciences & Oeschger Centre for Climate Change Research, University of Bern, Bern, 3012, Switzerland

^d Research Institute for Health Sciences (RIHES), Chiang Mai University, Chiang Mai 50200, Thailand

ARTICLE INFO

Handling Editor Adrian Covaci

Keywords:

Biomass burning
Southeast Asia
Latin Hypercube Sampling
Radiocarbon
Organic markers
Carbonaceous aerosols

ABSTRACT

Biomass burning (BB) is an important contributor to the air pollution in Southeast Asia (SEA), but the emission sources remain great uncertainty. In this study, PM_{2.5} samples were collected from an urban (Chiang Mai University, CMU) and a rural (Nong Tao village, NT) site in Chiang Mai, Thailand from February to April (high BB season, HBB) and from June to September (low BB season, LBB) in 2018. Source apportionment of carbonaceous aerosols was carried out by Latin Hypercube Sampling (LHS) method incorporating the radiocarbon (¹⁴C) and organic markers (e.g., dehydrated sugars, aromatic acids, etc.). Thereby, carbonaceous aerosols were divided into the fossil-derived elemental carbon (EC_f), BB-derived EC (EC_{bb}), fossil-derived primary and secondary organic carbon (POC_f, SOC_f), BB-derived OC (OC_{bb}) and the remaining OC (OC_{nf, other}). The fractions of EC_{bb} generally prevailed over EC_f throughout the year. OC_{bb} was the dominant contributor to total carbon with a clear seasonal trend (65.5 ± 5.8 % at CMU and 79.9 ± 7.6 % at NT in HBB, and 39.1 ± 7.9 % and 42.8 ± 4.6 % in LBB). The distribution of POC_f showed a spatial difference with a higher contribution at CMU, while SOC_f displayed a temporal variation with a greater fraction in LBB. OC_{nf, other} was originated from biogenic secondary aerosols, cooking emissions and bioaerosols as resolved by the principal component analysis with multiple linear regression model. The OC_{nf, other} contributed within a narrow range of 6.6 %-14.4 %, despite 34.9 ± 7.9 % at NT in LBB. Our results highlight the dominance of BB-derived fractions in carbonaceous aerosols in HBB, and call the attention to the higher production of SOC in LBB.

1. Introduction

Biomass burning (BB) is defined as the combustion of plant matter in open fires and as biofuels (Li et al., 2021). BB can affect the air quality (Bo et al., 2008), the regional/global climate (Li et al., 2003; Myhre et al., 2013), and are strongly correlated with negative health effects (Marlier et al., 2013; Reddington et al., 2015).

Around 15 % of the world's tropical forests are distributed in Southeast Asia (SEA), normally including Myanmar, Thailand, Laos, Cambodia and Vietnam). Large scale BB in SEA are performed annually in the dry season (February-April) (Gautam et al., 2013; Jian & Fu, 2014; Koplitz et al., 2017; Tsay et al., 2013). A number of studies concerned the BB-derived air pollution in SEA have been conducted. In general, BB

dominates the air pollution and peaks in March in this area. Specifically, forest fire prevails over agricultural residue burning (ARB), and rice straw burning is pronounced in ARB emissions. Notably, BB aerosols originated from SEA can affect downwind areas, e.g., Southern China and northwestern Pacific (Deng et al., 2008; Huang et al., 2019; Jian & Fu, 2014; Lee et al., 2011; Sheu et al., 2010; Zheng et al., 2018), Malay Archipelago (Bagtasa et al., 2019; Dotse et al., 2016; Liang et al., 2019) and even further to North America (Peltier et al., 2008). The molecular tracers, diagnostic ratios, Positive Matrix Factorization (PMF) model, Principal Component Analysis (PCA) and stable isotopes (δ¹³C, δ¹⁵N) are the main methods used to do the aerosol source apportionment in SEA (Boreddy et al. 2018a, 2018b; Chansuebsri et al. 2022; Choochuay et al. 2020a; ChooChuay et al. 2020b; Chuang et al. 2013; Kawichai et al.

* Corresponding author.

E-mail address: zhangyanlin@nuist.edu.cn (Y.-L. Zhang).

<https://doi.org/10.1016/j.envint.2022.107466>

Received 7 June 2022; Received in revised form 3 August 2022; Accepted 9 August 2022

Available online 13 August 2022

0160-4120/© 2022 The Authors. Published by Elsevier Ltd. This is an open access article under the CC BY-NC-ND license (<http://creativecommons.org/licenses/by-nc-nd/4.0/>).

2020; Phairuang et al. 2019; Pongpiachan et al., 2017; Tsai et al. 2013; Yin et al. 2019; Zheng et al. 2018).

Previous studies in SEA were mostly concerned the haze episodes in high BB season (HBB), however, there is still discrepancy between the observed $PM_{2.5}$ concentration and the air quality guideline ($5 \mu g m^{-3}$) by World Health Organization (WHO) even in low BB season (LBB). This campaign covered both HBB and LBB to uncover the emission sources besides BB.

Vehicular emission (VE) is another important contributor to the air pollution in SEA. Choochuay et al (2020a, 2020b) found that VE was the greatest contributor to $PM_{2.5}$ in Phuket, Thailand. Kawichai et al (2020) demonstrated the important contribution from VE to the air pollution in Chiang Mai, Thailand. Fossil-fuel-powered two-wheeled vehicles (FPTWs) are widely used in SEA wherein Thailand ranks number 3 worldwide in terms of the ownership of FPTWs per 1000 population (Haworth, 2012). The motorcyclists are directly exposed to the vehicle exhaust which is undoubtedly harmful to human body, and the harm could be aggravated in traffic congestion due to the increment of the emission factors for exhaust emissions as well as the exposure time (Tet et al., 2002).

The traditional source apportionment methods are inevitably being subjectively influenced thus lessen the reliability of the results. And most of the previous works tended to study a specific class of the aerosols (e.g., PAHs, water soluble ions, etc.) which can hardly explain or on behalf of the overall $PM_{2.5}$. In our work, the bulk carbon in $PM_{2.5}$ was studied and the introduced radiocarbon (^{14}C) analysis can greatly reduce the uncertainties in source apportionment of carbonaceous aerosols because ^{14}C exists exclusively in non-fossil materials. The reason for fossil-fuels (FF) free from ^{14}C is that radiocarbon's half-life (~ 5730 years) is much shorter than the time required by the formation of FF. Accordingly, ^{14}C brings a better constrain for aerosol source apportionment comparing to the traditional methods mentioned above.

To the best of our knowledge, this is the first time ^{14}C used in the

aerosol study in SEA. The ^{14}C measurements were performed on total carbon (TC), elemental carbon (EC) and water-soluble organic carbon (WSOC) separately, which can better constrain the contributions from varied emission sources to different carbonaceous fractions and provide more insights into the air quality controlling strategies.

2. Method

2.1. Aerosol sampling

The collection of $PM_{2.5}$ samples were conducted at an urban site ($18.80^{\circ}N$, $98.96^{\circ}E$, 345 m, Chiang Mai University, CMU) and a rural site ($18.68^{\circ}N$, $98.55^{\circ}E$, 1016 m, Nong Tao village health center, NT) in Chiang Mai (shown in Fig. 1), Thailand during an HBB campaign (February to April 2018) and an LBB campaign (June to September 2018). The definition of HBB and LBB season is based on the number of hotspots. In this work, there were on average 69.8 and 0.1 hotspots per day during HBB and LBB in Chiang Mai province. The urban site is located in a basin and affected by multiple pollution sources including BB, traffic emissions, cooking emissions, etc. The rural site is located in a remote village surrounded by forest and farmland. The medium-volume air samplers (KC-120H, Qingdao Laoshan Co., Ltd, China) with a flow rate of $100 L min^{-1}$ were used to collect the $PM_{2.5}$ samples on pre-combusted ($450^{\circ}C$, 6 h) quartz filters (2500QAT-UP, Pall, diameter is 90 mm). After sampling, the filters were wrapped with aluminum foil papers separately and stored in the freezer at $-20^{\circ}C$ before analysis.

2.2. Chemical analysis

2.2.1. OC/EC analysis

The concentrations of OC and EC were analyzed by using an OC/EC analyzer (Model 4, Sunset Lab. Inc.; Oregon, USA). Filters with a diameter of 8.5 mm were punched out and analyzed in accordance with

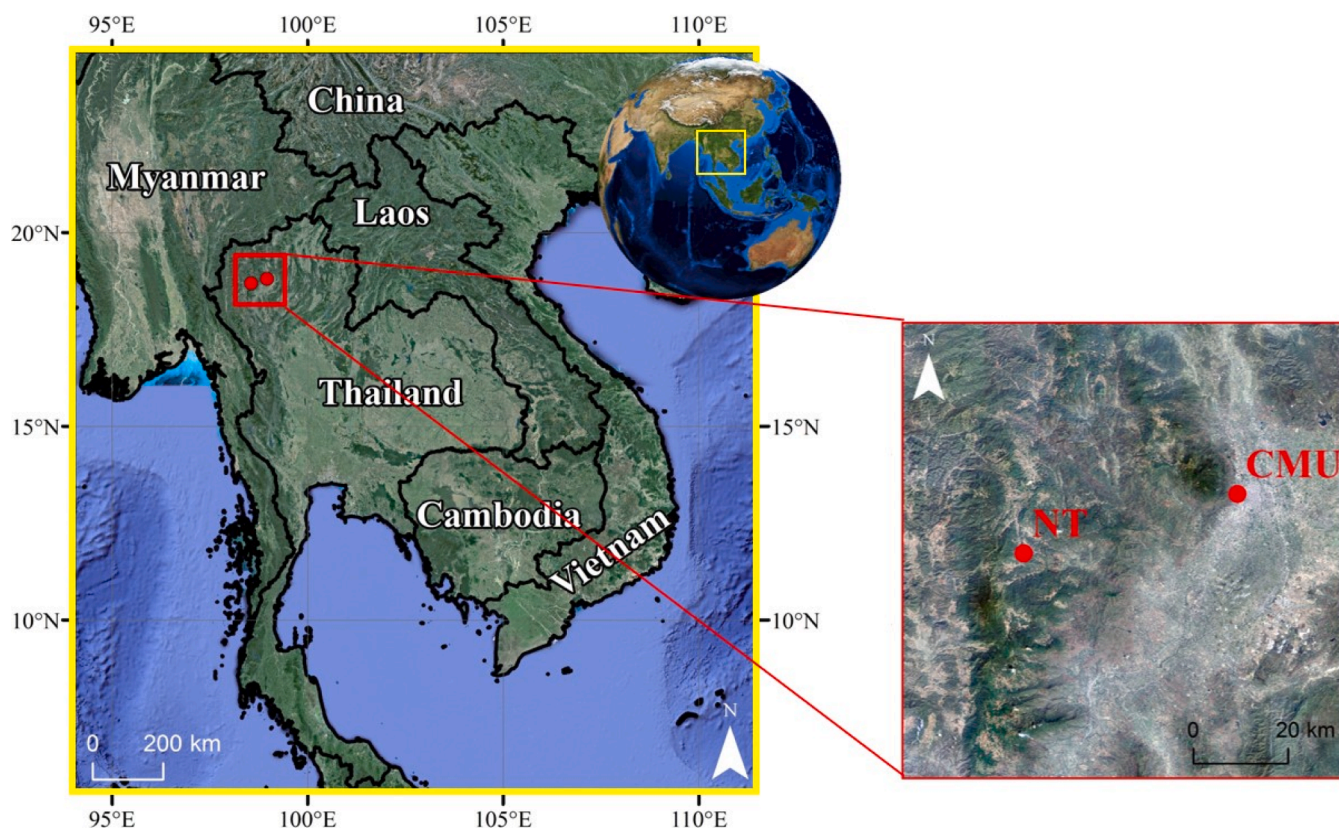


Fig. 1. Location of sampling sites. The image on the right was obtained from © Google Maps.

the NIOSH 5040 protocol (Lin et al., 2009).

2.2.2. Organic compounds

The organic compounds were determined by gas chromatography-mass spectrometry (GC-MS) system (GC7890B/MS5977A, Agilent Technologies; Santa Clara, CA). The filter aliquots were extracted with dichloromethane/methanol (2:1; v/v) under ultrasonication for 10 min and three times, and then being concentrated by using a sand bath and nitrogen sweeping. The extracts were then reacted with 50 μ L of N,O-bis-(trimethylsilyl)trifluoroacetamide (BSTFA) with 1 % trimethylsilyl chloride and 10 μ L of pyridine at 70 $^{\circ}$ C for 3 h prior to the GC-MS determination (Wu et al., 2020). The levoglucosan, mannosan, galactosan, erythritol, 2-methylglyceric acid, pinonic acid, pinic acid, β -caryophyllenic acid, and two saturated fatty acids (C_{16:0}, C_{18:0}) were analyzed in this work. Recoveries for the target compounds were better than 80 % as obtained by spiking standards to pre-combusted quartz filters followed by extraction and derivatization. Field blank filters were analyzed using the same procedure performed on the filter samples, and no target compounds could be detected. Duplicate analyses showed the analytical errors were less than 15 %.

Water-soluble ions: In this work, the water-soluble ions on the sample filters were measured by ion chromatography (IC, ICS 5000+, Thermo Scientific) after being extracted with ultra-pure water (Milli-Q Reference, America) under ultrasonication for 30 min. There are two systems for determining the cations (guard column: CG12A 4 mm; separation column: CS12A 4 mm) and anions (guard column: AG11 HC 4 mm; separation column: AS11 HC 4 mm) (Liu et al., 2019). Na⁺, NH₄⁺, K⁺, Mg²⁺, Ca²⁺, Cl⁻, NO₃⁻, SO₄²⁻, etc. were measured in this study.

2.3. Radiocarbon analysis

Thirty filters were selected for the ¹⁴C measurements (including T¹⁴C, E¹⁴C and WSO¹⁴C). Those filters were distributed over the whole campaign and their concentrations were close to that of the whole samples. The ¹⁴C of TC and EC were measured using a one-step protocol under pure O₂ (99.9995 %) at 760 $^{\circ}$ C for 400 s (Vlachou et al., 2018) using a Sunset OC/EC analyzer (Model 5L, Sunset Laboratory, USA) coupled with the accelerator mass spectrometer Mini Carbon Dating System (MICADAS) at the Laboratory for the Analysis of Radiocarbon (LARA; University of Bern) (Zhang et al., 2012; Szidat et al., 2014). Prior to the ¹⁴C measurement for EC, the filters were extracted with deionized water to remove the WSOC to minimize the positive artifact from OC charring, then the extracted solution was collected for ¹⁴C measurement of WSOC. After air drying in the fume hood, the extracted filters were thermally desorbed in the OC/EC analyzer with the use of the first three steps of the Swiss_4S protocol (Zhang et al., 2012) to isolate EC with EC yields of 74 % \pm 12 %. The workflow diagram for radiocarbon measurement is shown in Fig. S1 for reference. F¹⁴C(EC) was extrapolated to 100 % EC yield and corrected for pyrolyzed OC with a thermal-desorption model (Raubert and Salazar 2022, Raubert et al. 2022 (in prep.)). F¹⁴C(WSOC) was measured by chemical wet oxidation of the water extraction eluate (Raubert et al. 2022 (in prep.)). The ¹⁴C results are the modern fractions of the measured carbon (F¹⁴C), which is expressed as (Reimer et al., 2004):

$$F^{14}C = \left(\frac{{}^{14}C/{}^{12}C}{\text{sample}} \right) / \left(\frac{{}^{14}C/{}^{12}C}{1950} \right) \quad (1)$$

where $(\frac{{}^{14}C}{{}^{12}C})_{1950}$ is the reference isotopic ratio in 1950. In this study, ¹⁴C data analysis were carried out accounting for the charring of water-insoluble organic carbon (WINSOC) (~1 %), and EC yield after OC removal (CMU: 63.0 %-87.4 %; NT: 43.1 %-90.4 %) (Sönke Szidat et al., 2014; Zhang et al., 2012). In addition, the F¹⁴C values were corrected for the nuclear bomb in 1950 s by dividing the reference value ($f_{nf,ref}$) to obtain the non-fossil fractions (f_{nf}) of carbon:

$$f_{nf} = \frac{F^{14}C}{f_{nf,ref}} \quad (2)$$

As the modern carbon can come from BB and biogenic (bio) sources, the $f_{nf,ref}$ should be divided into $f_{bb,ref}$ and $f_{bio,ref}$, wherein $f_{bb,ref}$ is calculated by a tree-growth model (Mohn et al., 2008). In this study, $f_{bb,ref}$ (1.11) and $f_{bio,ref}$ (1.01) were set as the upper and lower limits of $f_{nf,ref}$, and the median value of them (1.06) was set as the middle value of $f_{nf,ref}$ (details of the calculation is described in Supplement).

$$f_{nf}(TC) = \frac{F^{14}C(TC)}{f_{nf,ref}} \quad (3)$$

$$TC_{nf} = TC \times f_{nf}(TC) \quad (4)$$

Given non-fossil EC is exclusively from BB, the correction formula for $f_{nf}(EC)$ could be expressed as follows:

$$f_{nf}(EC) = \frac{F^{14}C(EC)}{f_{nf,ref}} = \frac{F^{14}C(EC)}{f_{bb,ref}} \quad (5)$$

$$EC_{nf} = TC \times f_{nf}(EC) \quad (6)$$

Analogously, the non-fossil fraction of WSOC is calculated as follows:

$$f_{nf}(WSOC) = \frac{F^{14}C(WSOC)}{f_{nf,ref}} \quad (7)$$

$$WSOC_{nf} = WSOC \times f_{nf}(WSOC) \quad (8)$$

The non-fossil fractions of OC and WINSOC were calculated by following a mass-balance-like approach described in previous study (Hou et al., 2021):

$$OC_{nf} = TC_{nf} - EC_{nf} \quad (9)$$

$$WINSOC_{nf} = OC_{nf} - WSOC_{nf} \quad (10)$$

2.4. Source apportionment methodology

Zhang et al. (2015a, 2015b) introduced the LHS method in great detail, here it is described briefly. EC is emitted from the incomplete combustion of FF and NF sources:

$$EC = EC_f + EC_{nf} \quad (11)$$

Given that EC_{nf} is exclusively from BB (Hou et al. 2021; Zhang et al. 2015a, 2015b), the formula is modified as:

$$EC = EC_f + EC_{bb} \quad (12)$$

where EC_f is regarded entirely emitted by vehicles in the study area, and EC_{bb} is calculated by using the measured EC mass and $f_{nf}(EC)$ as follows:

$$EC_{bb} = EC \times f_{nf}(EC) \quad (13)$$

where $f_{nf}(EC)$ could be derived from equation (5). Analogously, OC could also be separated into FF and NF fractions:

$$OC = OC_f + OC_{nf} \quad (14)$$

where OC_{nf} is got from equation (9), and OC_f could be derived from (12) and (13). OC_f could be further divided into primary and secondary OC (POC_f and SOC_f) emitted from fossil-fuel combustion:

$$OC_f = POC_f + SOC_f \quad (15)$$

As FF sources in Chiang Mai is almost exclusively from vehicle emissions, they can be derived as follows:

$$POC_f \approx POC_{ve} = EC_{ve} \times (OC/EC)_{ve, pri} \quad (16)$$

wherein $(OC/EC)_{ve, pri}$ is a reference value of vehicle emissions (details

are in Table S1), EC_{ve} equals to EC_f .

$$OC_{nf} = OC_{bb} + OC_{nf, other} \quad (17)$$

where $OC_{nf, other}$ includes all the remaining non-fossil OC fractions other than from BB, e.g., biogenic and cooking emissions. OC_{bb} is derived as follows:

$$OC_{bb} = \frac{LG_{ori}}{LG/OC_{bb}} \quad (18)$$

wherein (LG/OC_{bb}) is a reference value of BB, and LG is the abbreviation of levoglucosan. It is noteworthy that LG will undergo distinct chemical degradation after being emitted (Y. Li et al., 2021), which means the ambient LG concentration cannot be directly used for calculation otherwise the contribution from biomass burning would be underestimated. In this study, the concentration of measured LG was calibrated to its theoretical original concentration (LG_{ori}) by using the following equation (Li et al., 2021):

$$LG = \frac{LG \times nss-K^+}{0.18LG + 0.08nss-K^+} \quad (19)$$

where LG and $nss-K^+$ are the concentrations of measured LG and non-sea-salt K^+ in the ambient air (Keene et al., 1986),

$$nss-K^+ = K^+ - 0.037Na^+ \quad (20)$$

where Na^+ is the concentration of measured Na^+ .

To evaluate the uncertainties introduced by the variables mentioned above, a random sampling model inspired by the Latin hypercube

sampling method (Gelencsér et al., 2007) was used. The variables varied within a range (Table S1), and the calculations were performed with 3000 random sets of variables. The negative simulated values were excluded and the median of the remaining simulations was considered as the best estimate.

2.5. Backward trajectories

The 48 h air-mass back-trajectories were calculated to study the influence of the regional transport. The calculations were carried out at the elevation of 345 m (at CMU) and 1016 m (at NT) above the sea level at 09:00 local time using the NOAA HYSPLIT model. The characteristics of air mass origins were determined by cluster analysis.

3. Results and discussion

3.1. Overall results

3.1.1. Characteristics of $PM_{2.5}$, OC, EC and organic compounds concentrations

Time series of the concentrations of $PM_{2.5}$, organic carbon (OC), elemental carbon (EC), number of hotspots and meteorological parameters (including temperature, relative humidity, precipitation) are plotted in Fig. 2 and summarized in Table 1. The average concentrations of $PM_{2.5}$ were $55.5 \pm 20.1 \mu\text{g m}^{-3}$ and $48.5 \pm 23.3 \mu\text{g m}^{-3}$ at CMU and NT in HBB, $14.7 \pm 7.5 \mu\text{g m}^{-3}$ and $7.0 \pm 2.5 \mu\text{g m}^{-3}$ in LBB, respectively. The highest level of $PM_{2.5}$ was $88.8 \mu\text{g m}^{-3}$ (CMU) and $103.1 \mu\text{g m}^{-3}$ (NT), and there were 13 out of 23 and 12 out of 25 observational days

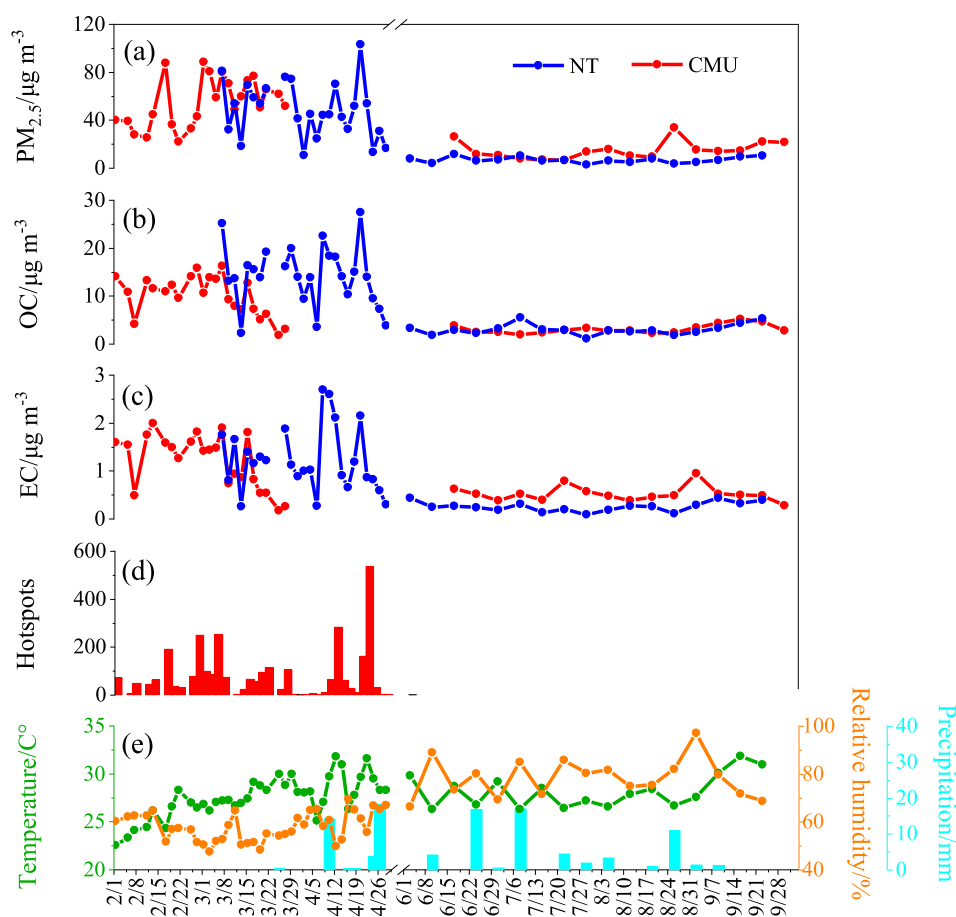


Fig. 2. Time series of the concentration of chemical species measured on the collected sampling filters, as well as the hotspots and meteorological data. (a) $PM_{2.5}/\mu\text{g m}^{-3}$; (b) $OC/\mu\text{g m}^{-3}$; (c) $EC/\mu\text{g m}^{-3}$ (d) the number of hotspots in Chiang Mai province (requested from <https://firms.modaps.eosdis.nasa.gov>) and (e) temperature/ $^{\circ}\text{C}$, relative humidity (RH) and precipitation/mm. The meteorological data are from the AQM station in Chiang Mai (18.78°N 98.99°E).

Table 1

Concentrations of carbonaceous aerosols, inorganic ions and organic tracers, as well as the diagnostic ratios and modern fractions of carbonaceous aerosols ($F^{14}C$) for the campaign.

Parameters	CMU		NT	
	Mean \pm sd (min–max)	Mean \pm sd (min–max)	Mean \pm sd (min–max)	Mean \pm sd (min–max)
Sampling period	2018.2.2–2018.3.28	2018.6.18–2018.9.24	2018.3.8–2018.4.29	2018.6.18–2018.9.24
PM_{2.5} ($\mu\text{g m}^{-3}$)	55.5 \pm 20.1 (22.1–88.8)	14.7 \pm 7.5 (6.7–33.7)	48.5 \pm 23.3 (10.7–103.1)	7.0 \pm 2.5 (2.9–11.6)
TC ($\mu\text{g m}^{-3}$)	11.4 \pm 4.7 (2.1–20.0)	3.7 \pm 1.0 (2.5–5.7)	25.6 \pm 10.7 (3.5–44.2)	3.3 \pm 1.2 (1.3–5.8)
TC_{nf} ($\mu\text{g m}^{-3}$)	11.0 \pm 4.8 (1.5–16.3)	2.1 \pm 0.6 (1.3–3.2)	17.5 \pm 8.3 (3.5–25.8)	3.0 \pm 1.1 (1.6–5.2)
TC_f ($\mu\text{g m}^{-3}$)	1.9 \pm 0.8 (0.6–3.1)	1.5 \pm 0.4 (1.1–2.0)	1.4 \pm 0.9 (0.5–1.9)	0.5 \pm 0.1 (0.4–0.6)
OC ($\mu\text{g m}^{-3}$)	10.2 \pm 4.1 (1.9–18.8)	3.1 \pm 0.9 (2.0–5.2)	14.3 \pm 6.3 (2.3–27.5)	3.1 \pm 1.1 (1.2–5.5)
OC_{nf} ($\mu\text{g m}^{-3}$)	10.3 \pm 4.5 (1.3–15.0)	1.8 \pm 0.5 (1.2–2.4)	16.2 \pm 7.9 (3.4–26.0)	2.7 \pm 0.8 (2.2–3.9)
OC_f ($\mu\text{g m}^{-3}$)	1.2 \pm 0.4 (0.6–1.7)	1.2 \pm 0.3 (1.0–1.6)	1.1 \pm 1.2 (0.3–3.6)	0.5 \pm 0.0 (0.4–0.5)
EC ($\mu\text{g m}^{-3}$)	1.2 \pm 0.6 (0.2–2.0)	0.5 \pm 0.2 (0.3–0.9)	1.2 \pm 0.7 (0.3–2.7)	0.3 \pm 0.1 (0.1–0.4)
EC_{nf} ($\mu\text{g m}^{-3}$)	1.1 \pm 0.5 (0.2–1.6)	0.3 \pm 0.1 (0.2–0.6)	1.3 \pm 0.6 (0.2–2.0)	0.3 \pm 0.1 (0.2–0.3)
EC_f ($\mu\text{g m}^{-3}$)	0.4 \pm 0.2 (0.0–0.7)	0.3 \pm 0.1 (0.2–0.4)	0.2 \pm 0.1 (0.1–0.3)	0.0 \pm 0.0 (0.0–0.1)
(OC/EC)_{nf}	9.4 \pm 1.5 (11.6–7.7)	7.5 \pm 3.5 (4.5–12.4)	12.9 \pm 2.9 (9.0–17.3)	11.1 \pm 4.2 (7.5–16.4)
(OC/EC)_f	3.2 \pm 0.8 (2.4–4.2)	4.7 \pm 1.0 (3.3–5.6)	3.6 \pm 2.5 (1.4–7.7)	14.6 \pm 10.8 (8.6–30.8)
WSOC ($\mu\text{g m}^{-3}$)	8.0 \pm 3.4 (1.3–12.5)	1.7 \pm 0.8 (0.8–3.5)	11.3 \pm 5.3 (1.2–20.3)	1.2 \pm 0.6 (0.4–2.8)
WSOC_{nf} ($\mu\text{g m}^{-3}$)	8.6 \pm 3.8 (0.9–12.0)	1.0 \pm 0.4 (0.5–1.7)	11.6 \pm 5.8 (1.5–18.7)	0.9 \pm 0.4 (0.4–1.4)
WSOC_f ($\mu\text{g m}^{-3}$)	0.7 \pm 0.4 (0.3–1.4)	0.6 \pm 0.2 (0.4–0.9)	0.7 \pm 0.9 (0.2–2.6)	0.4 \pm 0.1 (0.3–0.6)
WINSOC ($\mu\text{g m}^{-3}$)	2.3 \pm 1.2 (0.6–9.1)	1.4 \pm 0.4 (0.6–2.1)	3.7 \pm 3.0 (0.8–15.6)	1.9 \pm 0.8 (0.4–4.1)
WINSOC_{nf} ($\mu\text{g m}^{-3}$)	1.7 \pm 1.0 (0.4–2.9)	0.8 \pm 0.3 (0.5–1.0)	4.7 \pm 4.5 (1.9–14.5)	1.9 \pm 0.9 (1.4–3.2)
WINSOC_f ($\mu\text{g m}^{-3}$)	0.4 \pm 0.3 (0.2–1.0)	0.7 \pm 0.2 (0.5–0.9)	0.4 \pm 0.5 (0.1–1.2)	0.1 \pm 0.0 (0.1–0.1)
(WINSOC/EC)_{nf}	1.7 \pm 0.7 (0.7–2.8)	3.5 \pm 2.1 (1.8–6.5)	4.1 \pm 2.8 (1.2–7.8)	7.7 \pm 4.2 (4.5–13.4)
(WINSOC/EC)_f	1.2 \pm 0.9 (0.4–2.9)	2.6 \pm 0.7 (1.6–3.3)	2.0 \pm 1.9 (0.4–4.5)	2.7 \pm 2.9 (0.9–7.0)
WSOC_{nf}/(WSOC + EC)_{nf}	3.1 \pm 1.1 (1.6–4.7)	0.9 \pm 0.1 (0.8–0.9)	2.4 \pm 1.5 (0.7–4.2)	0.5 \pm 0.2 (0.2–0.6)
WSOC_f/(WSOC + EC)_f	1.1 \pm 0.8 (0.3–2.6)	0.4 \pm 0.2 (0.3–0.6)	1.2 \pm 0.9 (0.2–2.3)	3.4 \pm 0.5 (3.0–4.0)
F¹⁴C (TC)	0.80 \pm 0.11 (0.57–0.89)	0.59 \pm 0.06 (0.49–0.67)	0.91 \pm 0.06 (0.79–0.97)	0.86 \pm 0.04 (0.77–0.89)
F¹⁴C (OC)	0.81 \pm 0.10 (0.62–0.90)	0.59 \pm 0.06 (0.53–0.65)	0.91 \pm 0.07 (0.79–0.98)	0.87 \pm 0.01 (0.86–0.88)
F¹⁴C (EC)	0.70 \pm 0.18 (0.28–0.83)	0.57 \pm 0.01 (0.56–0.58)	0.84 \pm 0.05 (0.78–0.94)	0.86 \pm 0.08 (0.78–0.94)
F¹⁴C (WSOC)	0.80 \pm 0.21 (0.42–0.97)	0.64 \pm 0.08 (0.51–0.75)	0.89 \pm 0.12 (0.71–0.99)	0.65 \pm 0.08 (0.52–0.79)
F¹⁴C (WINSOC)	0.76 \pm 0.10 (0.59–0.89)	0.54 \pm 0.04 (0.51–0.58)	0.94 \pm 0.06 (0.80–1.01)	0.95 \pm 0.01 (0.95–0.97)
K⁺ ($\mu\text{g m}^{-3}$)	0.7 \pm 0.4 (0.1–1.3)	0.2 \pm 0.1 (0.1–0.4)	1.1 \pm 0.6 (0.1–2.0)	0.1 \pm 0.0 (0.0–0.2)
Lev (ng m^{-3})	396.4 \pm 219.5 (57.1–839.6)	51.6 \pm 24.2 (20.4–107.2)	991.6 \pm 578.9 (79.9–2489.9)	134.9 \pm 125.6 (5.2–485.7)
MN (ng m^{-3})	38.0 \pm 20.9 (4.8–83.6)	5.2 \pm 2.5 (2.2–10.8)	93.2 \pm 92.6 (5.8–499.0)	10.7 \pm 12.5 (0.0–51.4)
GA (ng m^{-3})	17.1 \pm 8.9 (2.5–37.6)	2.0 \pm 1.2 (0.6–4.6)	44.1 \pm 35.4 (2.6–186.5)	4.8 \pm 4.8 (0.0–18.7)

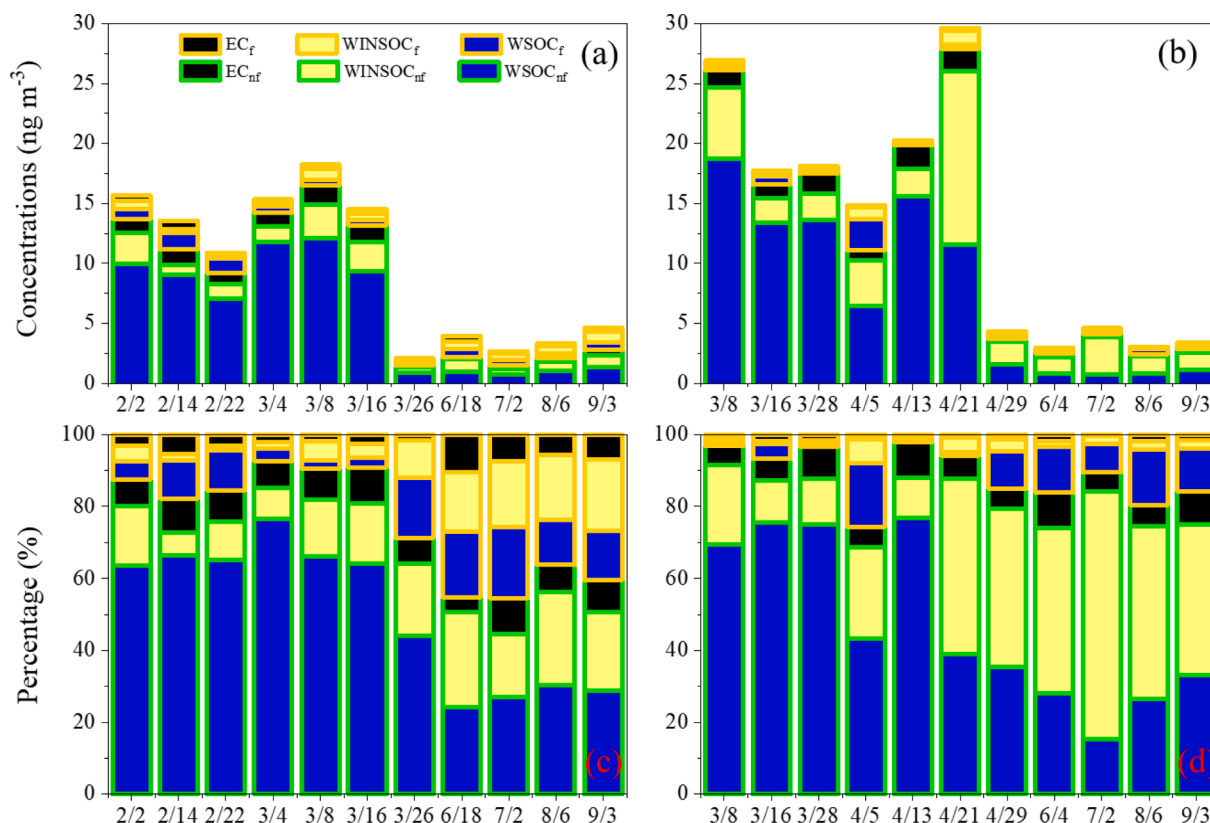


Fig. 3. Fossil- and non-fossil-derived carbon distinguished by ^{14}C results. (a) and (b) show the time series of the concentrations of fossil/non-fossil-derived EC, WINSOC as well as WSOC; (c) and (d) display their contributions to TC.

exceeding the Thailand daily air quality standard ($50 \mu\text{g m}^{-3}$) at CMU and NT during HBB, respectively. Carbonaceous aerosol was the dominant contributor to $\text{PM}_{2.5}$, wherein the total carbon (TC) accounted for $24.1 \pm 15.1\%$ and $35.3 \pm 18.3\%$ of $\text{PM}_{2.5}$ at CMU and NT in HBB and $28.3 \pm 10.9\%$ and $48.7 \pm 7.8\%$ in LBB, respectively. The strong correlations between OC and EC were found at both sites (shown in Fig. S2). The concentrations of TC, OC, EC, WSOC and WINSOC are displayed Table 1.

3.1.2. The contributions of fossil and non-fossil sources to different fractions of TC

The concentrations of the determined carbonaceous fractions and their contributions to TC are displayed in Fig. 3. EC_f mainly refers to vehicle emissions, and EC_{nf} is from biomass burning (Andrew and Cass 1998). The average concentrations of EC_f were $0.36 \pm 0.20 \mu\text{g m}^{-3}$ and $0.22 \pm 0.10 \mu\text{g m}^{-3}$ at CMU and NT sites in HBB, and $0.28 \pm 0.11 \mu\text{g m}^{-3}$, and $0.04 \pm 0.02 \mu\text{g m}^{-3}$ in LBB. Higher concentrations of EC_f were found in the urban site, which contributed 3% and 8% to TC in HBB and LBB, respectively. Meanwhile, EC_f accounted for only 0.1% to TC at the rural site in both HBB and LBB, suggesting that the primary vehicle emissions can hardly affect the air quality in rural areas. Fractions of EC_{nf} varied from 64.5% to 83.3%, 77.5% to 94.3% at CMU and NT in HBB, and from 27.9% to 58.1%, 77.6% to 94.0% in LBB, which are higher than previous studies conducted in Xi'an ($17 \pm 5\%$) (Ni et al., 2018), Budapest ($\sim 34.5\%$) (Salma et al., 2017), California ($48 \pm 8\%$) (Yoon et al., 2018), Beijing (9–30%) (Zhang et al. 2015a, 2015b), Oslo (30–40% in winter, 10–20% in summer) (Yttri et al., 2011), Guangzhou ($20 \pm 5\%$) (Liu et al., 2016). The concentrations of EC_{nf} in HBB was 4.0 (CMU) and 5.0 times (NT) higher than that in LBB, indicating the elevated emissions of primary non-fossil sources during HBB, which is consistent with the intensive open biomass burning activities in this period of time in Thailand (Pani et al., 2018; Phairuang et al., 2019).

As coal combustion contributed little to the aerosol particles in Thailand (Chansuebsri et al., 2022; Pongpiachan et al., 2017; Yin et al., 2019), the fossil-OC (OC_f) was mainly originated from vehicle emissions, while non-fossil-OC (OC_{nf}) was emitted mainly by biomass burning, biogenic emission, cooking, etc. Non-fossil sources were the dominant contributor to OC (accounted for $62.5 \pm 10.2\%$, $70.6 \pm 13.0\%$ at CMU and NT in HBB, and $38.5 \pm 7.9\%$, $43.4 \pm 4.6\%$ in LBB), especially in HBB. These results are higher than other studies conducted in four major cities in China ($55 \pm 10\%$) (Zhang et al. 2015a, 2015b), western arctic ($\sim 62\%$) (Barrett et al., 2015), Beijing ($52 \pm 12\%$) (Y. Zhang et al., 2017), Budapest ($\sim 68.2\%$) (Salma et al., 2017) and are comparable to an Alpine valley ($75 \pm 24\%$) (Vlachou et al., 2018). Given the cooking-derived OC_{nf} is roughly invariable within a year, the enhancement of OC_{nf} in HBB could be attributed to the intensive biomass burning activities as well as the biogenic emissions (including both POC and SOC).

The fossil and non-fossil fractions of WSOC and WINSOC were quantified in this study. In HBB, WSOC_{nf} were the greatest contributor to TC ($63.7 \pm 9.8\%$ at CMU and $59.4 \pm 18.7\%$ at NT), and followed by WINSOC_{nf} ($13.6 \pm 5.1\%$ at CMU and $25.4 \pm 15.9\%$ at NT). The dominance of WSOC_{nf} probably implies the great impact from biomass burning and/or the secondary formation process. In LBB, the contributions of WSOC_{nf} ($27.7 \pm 2.3\%$) were slightly higher than WINSOC_{nf} ($23.2 \pm 4.4\%$) at CMU, while WINSOC_{nf} became the most dominant contributor ($51.7 \pm 11.3\%$) followed by WSOC_{nf} ($26.1 \pm 7.9\%$) at NT. We suspect that the changes of weather conditions as well as the emission sources explain the increased contribution of water-insoluble fraction in LBB. These results are different from a previous study conducted in Beijing, in which WINSOC_f was the most abundant fraction of OC with an average contribution of around 40% (Hou et al., 2021). Furthermore, both WSOC and WINSOC were dominated by non-fossil fractions, WSOC_{nf} contributed $89.3 \pm 8.7\%$ and $90.9 \pm 11.7\%$ to WSOC at CMU and NT in HBB, decreased to $62.8 \pm 8.0\%$ and $66.6 \pm 8.5\%$ in LBB, and WINSOC_{nf} accounted for $78.7 \pm 7.2\%$, $92.3 \pm 5.8\%$ to WINSOC at CMU and NT in HBB, and $55.5 \pm 5.7\%$ and $95.9 \pm 1.0\%$

in LBB. Compared with reported results: non-fossil fractions contributed $74 \pm 8\%$, $51 \pm 2\%$ and 59% to WINSOC in Beijing, Guangzhou and a background site at the eastern coast of China (Liu et al., 2013; Liu et al., 2016), while $46 \pm 13\%$ and $60 \pm 11\%$ WSOC was derived from non-fossil sources in Beijing and Guangzhou (Liu et al., 2016). As discussed above, non-fossil derived WSOC and WINSOC made a pronounced contribution to carbonaceous aerosols in this study, however, the specific contributions from biomass burning and other contemporary sources haven't been specifically identified so far, the further discussion would be showed in detail in Section 3.2.

3.1.3. The contributions of certain carbonaceous aerosols to fossil and non-fossil fractions

In general, WSOC was the dominant contributor, especially to C_{nf} (non-fossil derived carbon), while WINSOC accounted for more in C_f (fossil derived carbon) than in C_{nf} , except at NT in LBB as shown in Fig. 4 (a). The results can be partially explained by that fossil-derived OC are more likely to be assigned to water insoluble portions, conversely, the non-fossil-derived OC tends to be water soluble (Mayol-Bracero et al. 2002; Weber et al. 2007; Wozniak et al. 2012a, 2012b; Zhang et al. 2013). The ratio of OC/EC are widely used in aerosol source apportionment, and it has been found that the biomass burning related sources are generally with higher OC/EC values than the fossil-fuel derived ones (Choochuay et al., 2020a, 2020b). In this study, $(\text{OC}/\text{EC})_{nf}$ are generally higher than $(\text{OC}/\text{EC})_f$ as displayed in Fig. 4(b), and details are shown in Table 1. It is noteworthy that the ratio of $(\text{OC}/\text{EC})_f$ at NT in LBB was significantly higher than the other fossil OC/EC values, and was comparable to the non-fossil OC/EC values. Boreddy (Boreddy et al. 2018a, 2018b) reported that the secondary formation could lead to high values of OC/EC (~ 21 to 33), Saarikoski (Saarikoski et al., 2008) recorded the high OC/EC value (12) observed in the long range transported aerosols as well. To study the influence of regional transport, back trajectories are plotted in Fig S3. The air masses at the sampling sites in HBB mostly originated from Myanmar and the neighboring cities in northern Thailand. While the sampling sites were more affected by the regional transport in LBB as the air masses mainly originated from the ocean and passed over southern Myanmar before arriving at the upper northern Thailand. Moreover, the low contribution of WINSOC_f and EC_f at NT in LBB demonstrated the decline of primary fossil sources, and the LHS results (find in Sect. 3.2.2) further supported the importance of SOC_f at NT in LBB. Accordingly, the high OC/EC values cannot be confidently linked to non-fossil emissions as it can also be resulted by the aged process and long-range transport.

As a result of the increased contribution of WINSOC_{nf} , the ratios of $(\text{WINSOC}/\text{EC})_{nf}$ were roughly-two times higher in LBB than in HBB at both NT and CMU sites. Specifically, the contribution of WINSOC_{nf} was higher than that of WSOC_{nf} at NT in LBB, and notably, $\text{F}^{14}\text{C}(\text{WINSOC})$ was $>\text{F}^{14}\text{C}(\text{WSOC})$ (see in Table 1), which is opposed to the majority of previous studies (Hou et al. 2021; Szidat et al. 2004; Wozniak et al., 2012a, 2012b; Zhang et al. 2013). Nonetheless, Zhang et al. (2014) just found the similar trend in Hainan Island in China and attributed to the large contribution from biomass burning to both WSOC and WINSOC. In this study, the mean values of $(\text{WINSOC}/\text{EC})_f$ were 1.2 (in HBB) and 2.6 (in LBB) at CMU, and 1.9 (in HBB) and 2.7 (in LBB) at NT, which are comparable to the reported results observed in East China (1.1–2.5) (D. Liu et al., 2013), Beijing (2.4) and Shanghai (1.3) (D. Liu et al., 2020). Generally, the WINSOC/EC ratios are higher in non-fossil sources than in fossil ones which is consistent with the finding by Liu (D. Liu et al., 2013).

To better understand the contributions from water soluble and insoluble fractions, the ratios of WSOC (WS) versus WINSOC plus EC (WINS) were calculated in this study and displayed in Fig. 4(c). The mean values of $(\text{WS}/\text{WINS})_{nf}$ were 3.4 and 2.7 at CMU and NT in HBB, and were 0.9 and 0.5 in LBB. The discrepancy of $(\text{WS}/\text{WINS})_{nf}$ probably indicates the BB-derived OC are more likely to be WS compared with other non-fossil OC. The fossil WS/WINS ratios were close to 1 with the

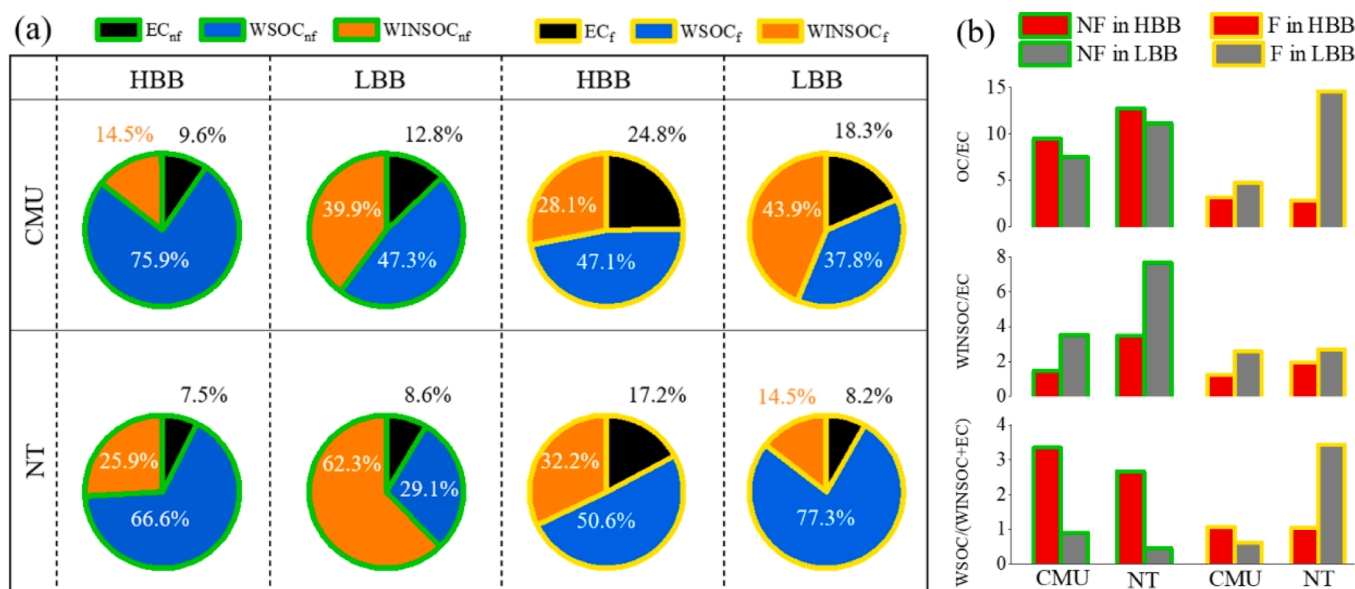


Fig. 4. The compositions and related ratios of fossil derived carbon (C_f , displayed with green border) and non-fossil derived carbon (C_{nf} , displayed with yellow border). (a) The contributions of EC, WSOC and WINSOC to C_f and C_{nf} , respectively; (b) The ratios of OC versus EC, WINSOC versus EC as well as WSOC versus WINSOC plus EC in C_f and C_{nf} , respectively. (For interpretation of the references to color in this figure legend, the reader is referred to the web version of this article.)

exception of 3.4 at NT in LBB (details are shown in Table 1). Similar to the high values of $(OC/EC)_f$, the decline of the contribution from primary fossil sources as well as the aged process and/or secondary formation possibly bring the high $(WS/WINS)_f$ values at NT in LBB.

3.2. Source apportionment by Latin hypercube sampling method

3.2.1. Biomass burning

Levoglucosan (LG) as well as its two isomers mannosan (MN) and galactosan (GA) are widely used as the tracers of BB as they are mainly produced from celluloses and hemicelluloses via thermal decomposition (Simoneit et al. 1999; Suci, et al., 2019). The more intensive BB activity in rural area resulted in the higher concentrations of LG at NT site ($991.6 \pm 578.9 \mu\text{g m}^{-3}$ in HBB, $134.9 \pm 125.6 \mu\text{g m}^{-3}$ in LBB) which is close to the values observed in Northern Thailand before (Boreddy, et al., 2018b; Chuang et al., 2013; Tsai et al., 2013). And the concentration of LG was $396.4 \pm 219.5 \mu\text{g m}^{-3}$ in HBB and $51.5 \pm 24.2 \mu\text{g m}^{-3}$ in LBB at CMU

site. The ratios of LG/MN and LG/GA provide information to distinguish the certain types of biomass burning (Kawamura et al., 2012). The ratios of LG/MN and LG/GA measured in this study as well as obtained from literature research (Engling et al. 2009; Fine et al., 2004a, 2004b; Iinuma et al. 2007; Dos Santos et al., 2002; Schmidl et al. 2008; Sheesley et al. 2003; Sun et al. 2019; Zhang et al. 2007) are plotted in Fig. 5. As concluded in the previous work (Chuang et al., 2013), there is a boundary of LG/MN ratios at around 10 separating the softwood and hardwood etc. In general, the two pairs of ratios in this study were with a narrow range, wherein LG/MN ratios were 10.7 ± 1.3 at CMU and 12.1 ± 2.3 at NT in HBB, and 10.0 ± 1.0 and 14.6 ± 4.5 in LBB. The higher values of LG/MN ratios at NT site (significantly higher during HBB) are probably attributed to the more intensive burning of the crops straws with higher LG/MN ratio values (Chuang et al., 2013) in rural area. In this study, the ratios distributed within the range of softwood, hardwood, etc., suggesting both the softwood and hardwood contributing to the open fire in northern Thailand which has been documented by others

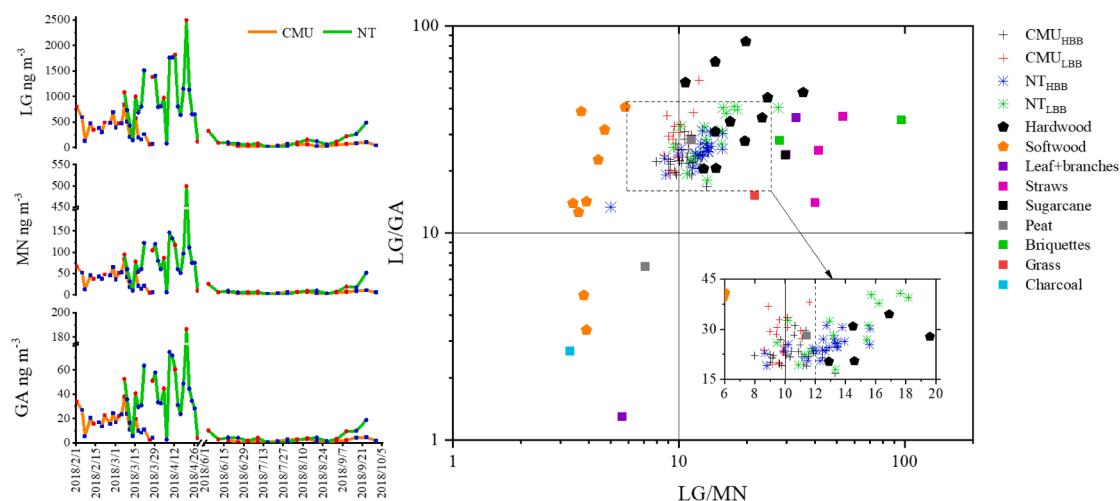


Fig. 5. The analysis of three dehydrated sugars. (a) Time series of the concentrations of LG, MN and GA at CMU and NT sites; (b) The diagnostic ratios of LG/MN versus LG/GA in this study as well as in the previously reported works.

(Boreddy et al. 2018a, 2018b; Chuang et al. 2013; Tsai et al. 2013; Zheng et al. 2018).

The concentration of LG multiplying the ratio of (LG/OC_{bb}) can derive OC_{bb} (Gelencsér et al., 2007), but the (LG/OC_{bb}) values can vary greatly with the change of the emission sources and the burning conditions thereby introducing the uncertainty. To determine a proper (LG/OC_{bb}) value, the dominant tree species were carefully selected according to the implication from dehydrated sugars mentioned above and the reported studies elsewhere (Chen 1994). The central value for (LG/OC_{bb}) is set at 0.28, and the detailed information are displayed in Sect 2.4. The frequency distribution of the different sources is displayed in Fig. 6, it is found that OC_{bb} was the largest contributor to TC and peaked at NT in HBB with the contributions of $70.6 \pm 13.0 \%$, and followed by $62.5 \pm 10.2 \%$ at CMU in HBB, $43.4 \pm 4.6 \%$ at NT in LBB, $38.5 \pm 7.9 \%$ at CMU in LBB. The difference between the 90th and 10th percentile of the solutions was used as an indicator of the uncertainty for the quantified emission sources. The OC_{bb} as well as OC_{other,nf} showed the greatest uncertainty due to the large variety of the input LG/OC_{bb} values mentioned above. The EC_f and EC_{bb} distributed within a narrower range compared to the sub-fractions of OC due to the direct ¹⁴C measurement for EC and the indirect calculation for OC.

3.2.2. Fossil-fuel emissions

Fossil-derived OC (OC_f, equals to the sum of POC_f and SOC_f) accounted for $11.2 \pm 7.4 \%$, $7.0 \pm 8.1 \%$ at CMU and NT in HBB, and

$33.5 \pm 2.9 \%$, $14.0 \pm 3.2 \%$ in LBB. The uncertainty of POC_f was equal to that of SOC_f (with the values of 3.3 % at CMU and 1.8 % at NT in HBB; 8.1 % at CMU and 1.8 % at NT in LBB) (displayed in Fig. 6). The highest uncertainty occurred at CMU site in HBB, which were associated with the lower concentration of carbonaceous aerosols in this season. Generally, the SOC_f were more abundant than POC_f, indicating that fossil-fuel emissions mainly affected the study area in the form of secondary aerosols, but CMU_{HBB} was an exception where primary fossil-fuel emissions contributed slightly more than secondary aerosols. Given that the vehicular emission (VE, the dominant contributor to fossil-fuel in the study area) remained roughly constant at sampling sites throughout a year, however, the concentration of OC_f reduced by around 30 % at NT in LBB ($0.7 \mu\text{g m}^{-3}$ in HBB, $0.5 \mu\text{g m}^{-3}$ in LBB) was observed as shown in Fig. 7(b). This reduction indicated the importance of long-range transport vehicular aerosol to NT site, as which had more chances to deposit during the transportation leading to the decrease of OC_f. The slighter reduction of OC_f was observed at CMU ($1.3 \mu\text{g m}^{-3}$ in HBB, $1.2 \mu\text{g m}^{-3}$ in LBB), implying the dominance of local vehicular emission sources in urban area. It is observed that the ratios of SOC_f/POC_f in LBB (2.3 ± 0.7 at CMU, 5.6 ± 0.7 at NT) were significantly higher than that in HBB (1.2 ± 0.6 at CMU, and 1.0 ± 1.1 at NT) at both two sites as shown in Fig. 7 (b). In this study, the RH was $58.3 \pm 6.1 \%$ during HBB and $78.6 \pm 6.0 \%$ during LBB, notably, the RH of 70 % split HBB and LBB as displayed in Fig. 7(a). It is reported that the formation of aqueous SOA (aqSOA) could be promoted under the conditions of RH being higher than 70 % (Ervens

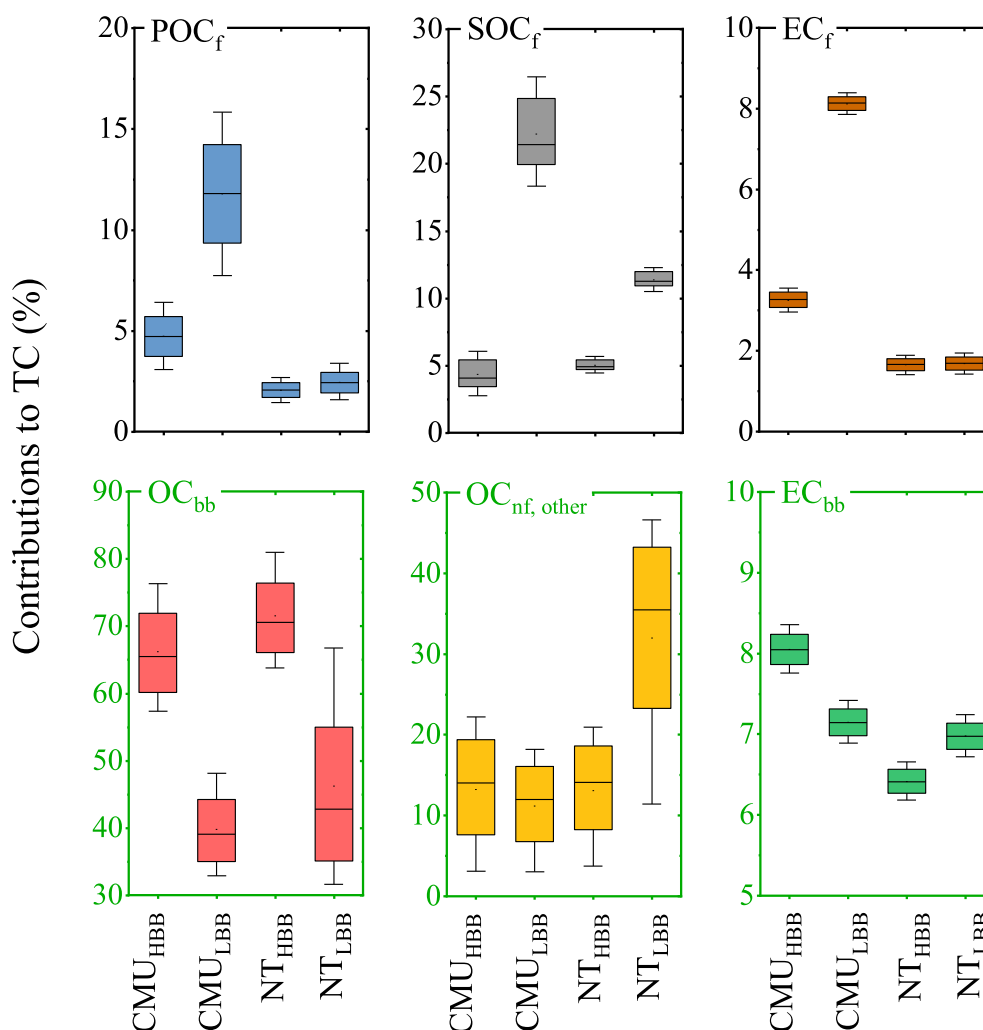


Fig. 6. Source apportionment of the carbonaceous aerosols by using LHS method. The box represents the 25th (lower line), 50th (middle line) and 75th (top line) percentiles; the end of the vertical bars represents the 10th (below the box) and 90th (above the box) percentiles.

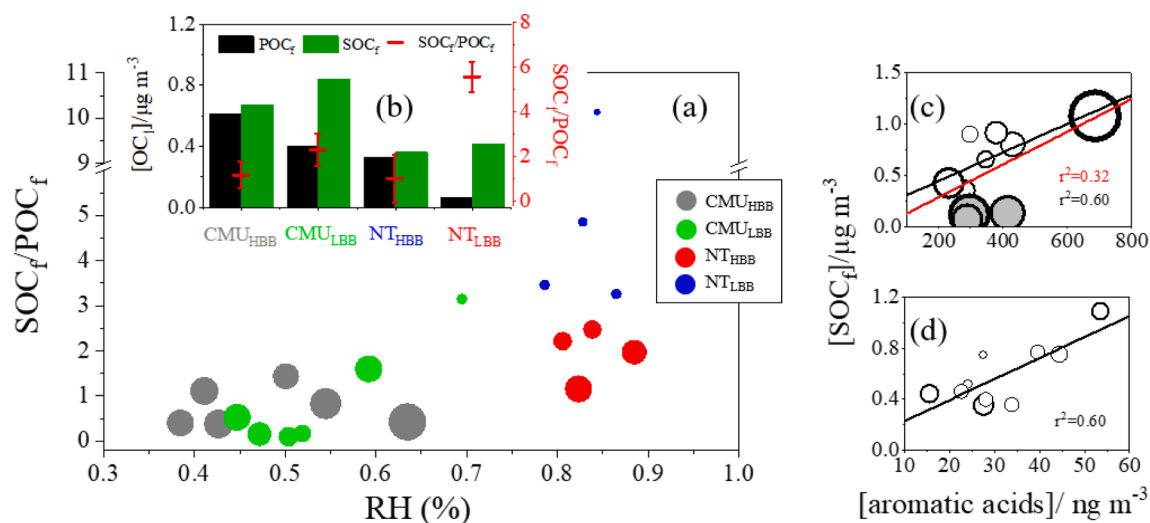


Fig. 7. Further analysis of the fossil derived OC. (a) The ratios of SOC_f/POC_f under different values of RH. The sizes of the circles indicate the amount of POC_f which ranges from 0.04 to 0.96 $\mu\text{g m}^{-3}$; (b) The mean concentrations of POC_f and SOC_f as well as the ratios of SOC_f/POC_f ; (c) and (d) show the correlation between SOC_f and the aromatic acids in HBB and LBB respectively, the sizes of the bubbles represent the concentration of OC_{bb} , note that the bubbles are with different scaling factors in (c) and (d) thus their sizes cannot be compared directly (the concentration of OC_{bb} in (c) ranges from 7.8 to 23.9 $\mu\text{g m}^{-3}$, and from 0.9 to 1.9 $\mu\text{g m}^{-3}$ in (d)).

et al., 2011). Whereby, the enhanced contribution of SOC_f during LBB was likely to be attributed to the more efficient generation of aqSOA under favorable RH condition. Certain types of vehicles, e.g., 2S scooters emit significant amount of aromatic VOC (volatile organic aerosol) (Platt et al., 2014), as there is no available VOC data, the aromatic acids (oxygenated from aromatic VOC) are used to surrogate the level as well as the variation of aromatic VOC (details are shown in Table S2). BB can also emit aromatic acids (Palm et al., 2020), which could explain the significantly higher amount of aromatic acids in HBB than in LBB. Pearson correlation coefficient (r^2) between SOC_f and aromatic acids in HBB is 0.32 (marked in red in Fig. 7(c)), and increases to 0.60 (marked in black) after excluding the three bubbles filled in gray color, which are with low level of SOC_f but high amounts of BB-derived aromatic acids. And the r^2 is 0.60 in LBB as shown in Fig. 7(d). The significantly strong correlation between SOC_f and aromatic acids suggests the aromatic VOCs to be the important precursors of SOC_f , and the lookout for the accompanying health risk should be kept. It should be noted that the more aged aerosols can pose severer health risk to human body, e.g., producing more reactive oxygen species (Lakey et al., 2016). Therefore, although OC_f remained unchanged or even decreased, the health risk caused by vehicle emissions should be paid closely attention in LBB as the SOC_f increased.

3.2.3. Other non-fossil emission sources

The principal component analysis-multiple liner regression (PCA-MLR) model is used to quantify the non-fossil sources other than BB. The following seven compounds: erythritol, 2-methylglyceric acid, pinonic acid, pinic acid, β -caryophyllenic acid, and two saturated fatty acids ($C_{16:0}$, $C_{18:0}$) were significantly correlated with $OC_{nf, other}$ (detailed information is in Table S2), whereby they were into a smaller set of liner combinations and extracted certain latent factors (principal components, PCs) with varimax rotation, the result is displayed in Table 2. Those selected compounds could be used as the surrogates for biogenic SOC (BSOC), primary biogenic aerosols (OC_{bio1}), and vascular plants-, microbial sources-, marine phytoplankton- as well as cooking-derived aerosols ($OC_{bio2+ck}$). Wherein, BSOC could be identified with 2-methylglyceric acid, pinonic acid, pinic acid and β -caryophyllenic acid, OC_{bio1} could be characterized by erythritol, $OC_{bio2+ck}$ is traced by $C_{16:0}$, $C_{18:0}$. Accordingly, $OC_{nf, other}$ were classified into two PCs. For CMU_{HBB} , NT_{HBB} and NT_{LBB} , PC1 explains the BSOC plus OC_{bio1} , PC2 explains $OC_{bio2+ck}$. And for CMU_{LBB} , PC1 explains BSOC, PC2 explains OC_{bio1} plus $OC_{bio2+ck}$ (marked as OC_{bio+ck}). Generally, $OC_{nf, other}$ accounted for near or less than 15 % with the exception of NT_{LBB} where $OC_{nf, other}$ contributed for more than 30 % to TC. The detailed information could be found in Table 2 as well as in the graphical abstract.

Table 2
Summary of factor loadings in PCA analysis over CMU and NT sites in HBB and LBB seasons.

Organic compounds	Component							
	CMU				NT			
	HBB		LBB		HBB		LBB	
	1	2	1	2	1	2	1	2
Erythritol	0.777	0.417	0.016	0.964	0.912	0.165	0.481	0.295
2-Methylglyceric acid	0.968	0.127	0.913	0.243	0.928	0.084	0.966	0.037
Pinonic acid	0.676	0.051	0.866	-0.006	0.207	0.712	0.408	0.777
Pinic acid	0.766	0.633	0.847	0.478	0.796	0.259	0.866	0.291
β -caryophyllenic acid	0.721	0.595	0.866	0.247	0.910	0.110	0.858	0.380
$C_{16:0}$	0.218	0.953	0.471	0.844	0.162	0.915	0.136	0.961
$C_{18:0}$	0.135	0.961	0.252	0.933	0.061	0.968	0.246	0.921
% of variance	44.5	34.0	47.7	40.8	46.1	34.2	41.4	38.5
% cumulative	44.5	78.5	47.7	88.5	46.1	80.3	41.2	79.8
% contributions to TC	7.7	7.6	5.1	7.7	8.6	5.7	15.7	17.8

4. Conclusions and implications

This study qualified the emission sources in different fractions of carbonaceous aerosols. By using ^{14}C analysis, less uncertainties were introduced to the source apportionment. Not surprisingly, BB is the greatest contributor to TC during HBB with the contributions of $63.8 \pm 9.0\%$ in urban area and $71.7 \pm 12.2\%$ in rural area and decreased to $40.4 \pm 7.3\%$ and $47.1 \pm 4.5\%$ in LBB, respectively. The contribution from vehicle-derived carbon was higher in LBB especially in urban area which accounted for $41.5 \pm 4.4\%$ to TC. Wherein SOC_f prevailed over POC_f in LBB, with the $\text{SOC}_f/\text{POC}_f$ ratios of 2.3 ± 0.7 in urban and 5.6 ± 0.7 in rural areas. As the aged aerosols tend to be more harmful to human body, e.g., generating more ROS and oxidative stress, the vehicle emissions in LBB should be paid closely attentions.

Additionally, it is widely accepted that compared to fossil-fuel derived aerosols, non-fossil-fuel derived aerosols are more likely to be water soluble and have higher OC/EC ratio values. However, these points seem to be unreliable when the long-range transport cannot be neglected. In this study, the higher contribution from SOA was observed in LBB especially at the rural site, wherein the OC_{nf} and OC_f contained 29.1% and 77.3% of WSOC respectively, meanwhile the fossil and non-fossil derived OC/EC ratios were 14.6 and 11.1, respectively.

From this study, BB is the main contributor to the air pollution throughout the year, thus the controlling of open fire is still of great importance. Notably, our work illuminated the necessity of restricting the VE, especially in LBB during when the high contribution from VE just coincides with the favorable RH for generating SOA which can thereby aggravate the health burden of the commuters. This implication is possibly applicable to a wider range in SEA, where the area is controlled by a tropical monsoon climate and the ownership of FPTWs is high.

CRedit authorship contribution statement

Wenhui Song: Investigation, Writing – original draft. **Yan-Lin Zhang:** Conceptualization, Supervision, Funding acquisition. **Yuxian Zhang:** Software. **Fang Cao:** Project administration. **Martin Rauber:** Methodology, Writing – review & editing, Writing – original draft. **Gary Salazar:** Methodology. **Sawaeng Kawichai:** Investigation. **Tippawan Prapamontol:** Funding acquisition. **Sönke Szidat:** Resources, Supervision.

Declaration of Competing Interest

The authors declare that they have no known competing financial interests or personal relationships that could have appeared to influence the work reported in this paper.

Data availability

Data will be made available on request.

Acknowledgments

This work was supported by the National Natural Science Foundation of China (grant numbers: 42192512, 41977305) and Thailand Science Research and Innovation (TSRI, formerly the Thailand Research Fund, TRF) (grant number: RDG 6030019). The authors would also like to thank the China Scholarship Council for the support to Wenhui Song.

Appendix A. Supplementary material

Supplementary data to this article can be found online at <https://doi.org/10.1016/j.envint.2022.107466>.

References

- Andrew Gray, H., Cass, G.R., 1998. Source contributions to atmospheric fine carbon particle concentrations. *Atmos. Environ.* 32 (22), 3805–3825. [https://doi.org/10.1016/S1352-2310\(97\)00446-9](https://doi.org/10.1016/S1352-2310(97)00446-9).
- Bagtasa, G., Cayetano, M.G., Yuan, C.S., Uchino, O., Sakai, T., Izumi, T., Morino, I., Nagai, T., Macatangay, R.C., Velasco, V.A., 2019. Long-range transport of aerosols from East and Southeast Asia to northern Philippines and its direct radiative forcing effect. *Atmos. Environ.* 218 (September), 117007 <https://doi.org/10.1016/j.atmosenv.2019.117007>.
- Barrett, T.E., Robinson, E.M., Usenko, S., Sheesley, R.J., 2015. Source contributions to wintertime elemental and organic carbon in the western arctic based on radiocarbon and tracer apportionment. *Environ. Sci. Technol.* 49 (19), 11631–11639. <https://doi.org/10.1021/acs.est.5b03081>.
- Bo, Y., Cai, H., Xie, S.D., 2008. Spatial and temporal variation of historical anthropogenic NMVOCs emission inventories in China. *Atmos. Chem. Phys.* 8 (23), 7297–7316. <https://doi.org/10.5194/acp-8-7297-2008>.
- Boreddy, S.K.R., Mozammel Haque, M., Kawamura, K., 2018a. Long-term (2001–2012) trends of carbonaceous aerosols from a remote island in the western North Pacific: an outflow region of Asian pollutants. *Atmos. Chem. Phys.* 18 (2), 1291–1306. <https://doi.org/10.5194/acp-18-1291-2018>.
- Boreddy, S.K.R., Parvin, F., Kawamura, K., Zhu, C., Lee, C.T., 2018b. Stable carbon and nitrogen isotopic compositions of fine aerosols (PM_{2.5}) during an intensive biomass burning over Southeast Asia: influence of SOA and aging. *Atmos. Environ.* 191 (August), 478–489. <https://doi.org/10.1016/j.atmosenv.2018.08.034>.
- Chansuebsri, S., Kraistinitikul, P., Wiriyaya, W., & Chantara, S., 2022. Chemosphere Fresh and aged PM 2.5 and their ion composition in rural and urban atmospheres of Northern Thailand in relation to source identification. 286(July 2021).
- Chen, X., 1994. Main types of forest vegetation in Thailand. *J. Tropical Subtropical Botany* 2 (1), 24–30.
- Choochuay, C., Pongpiachan, S., Tipmanee, D., Deelaman, W., Iadtem, N., Suttinun, O., Wang, Q., Xing, L.I., Li, G., Han, Y., Hashmi, M.Z., Palakun, J., Poshayachinda, S., Aukkaravittayapun, S., Surapipith, V., Cao, J., 2022. Effects of agricultural waste burning on PM_{2.5}-bound polycyclic aromatic hydrocarbons, carbonaceous compositions, and water-soluble ionic species in the ambient air of Chiang-Mai, Thailand. *Polycyclic Aromat. Compd.* 42 (3), 749–770.
- Choochuay, C., Pongpiachan, S., Tipmanee, D., Deelaman, W., Suttinun, O., Wang, Q., Xing, L., Li, G., Han, Y., Palakun, J., Poshayachinda, S., Aukkaravittayapun, S., Surapipith, V., Cao, J., 2020. Long-range Transboundary Atmospheric Transport of Polycyclic Aromatic Hydrocarbons, Carbonaceous Compositions, and Water-soluble Ionic Species in Southern Thailand. 1591–1606.
- Chuang, M.T., Chou, C.C.K., Sopajaree, K., Lin, N.H., Wang, J.L., Sheu, G.R., Chang, Y.J., Lee, C.T., 2013. Characterization of aerosol chemical properties from near-source biomass burning in the northern Indochina during 7-SEAS/Dongsha experiment. *Atmos. Environ.* 78, 72–81. <https://doi.org/10.1016/j.atmosenv.2012.06.056>.
- Deng, X., Tie, X., Zhou, X., Wu, D., Zhong, L., Tan, H., Li, F., Huang, X., Bi, X., Deng, T., 2008. Effects of Southeast Asia biomass burning on aerosols and ozone concentrations over the Pearl River Delta (PRD) region. *Atmos. Environ.* 42 (36), 8493–8501. <https://doi.org/10.1016/j.atmosenv.2008.08.013>.
- Dos Santos, C.Y.M., Azevedo, D.de A., De Aquino Neto, F.R., 2002. Selected organic compounds from biomass burning found in the atmospheric particulate matter over sugarcane plantation areas. *Atmos. Environ.* 36 (18), 3009–3019. [https://doi.org/10.1016/S1352-2310\(02\)00249-2](https://doi.org/10.1016/S1352-2310(02)00249-2).
- Dotse, S.Q., Dagar, L., Petra, M.I., De Silva, L.C., 2016. Influence of Southeast Asian Haze episodes on high PM₁₀ concentrations across Brunei Darussalam. *Environ. Pollut.* 219, 337–352. <https://doi.org/10.1016/j.envpol.2016.10.059>.
- Engling, G., Lee, J.J., Tsai, Y.W., Lung, S.C.C., Chou, C.C.K., Chan, C.Y., 2009. Size-resolved anhydrosugar composition in smoke aerosol from controlled field burning of rice straw. *Aerosol Sci. Technol.* 43 (7), 662–672. <https://doi.org/10.1080/02786820902825113>.
- Ervens, B., Turpin, B.J., Weber, R.J., 2011. Secondary organic aerosol formation in cloud droplets and aqueous particles (aqSOA): a review of laboratory, field and model studies. *Atmos. Chem. Phys.* 11 (21), 11069–11102. <https://doi.org/10.5194/acp-11-11069-2011>.
- Fine, P.M., Cass, G.R., Simoneit, B.R.T., 2004a. Chemical characterization of fine particle emissions from the fireplace combustion of wood types grown in the Midwestern and Western United States. *Environ. Eng. Sci.* 21 (3), 387–409. <https://doi.org/10.1089/109287504323067021>.
- Fine, P.M., Cass, G.R., Simoneit, B.R.T., 2004b. Chemical characterization of fine particle emissions from the wood stove combustion of prevalent united states tree species. *Environ. Eng. Sci.* 21 (6), 705–721. <https://doi.org/10.1089/ees.2004.21.705>.
- Gautam, R., Hsu, N.C., Eck, T.F., Holben, B.N., Janjai, S., Jantarach, T., Tsay, S.C., Lau, W.K., 2013. Characterization of aerosols over the Indochina peninsula from satellite-surface observations during biomass burning pre-monsoon season. *Atmos. Environ.* 78, 51–59. <https://doi.org/10.1016/j.atmosenv.2012.05.038>.
- Gelencsér, A., May, B., Simpson, D., Sánchez-Ochoa, A., Kasper-Giebl, A., Puxbaum, H., Caseiro, A., Pio, C.A., Legrand, M., 2007. Source apportionment of PM_{2.5} organic aerosol over Europe: primary/secondary, natural/anthropogenic, and fossil/biogenic origin. *J. Geophys. Res. Atmospheres* 112 (23). <https://doi.org/10.1029/2006JD008094>.
- Haworth, N., 2012. Powered two wheelers in a changing world - Challenges and opportunities. *Accid. Anal. Prev.* 44 (1), 12–18. <https://doi.org/10.1016/j.aap.2010.10.031>.
- Hou, S., Liu, D., Xu, J., Vu, T.V., Wu, X., Srivastava, D., Fu, P., Li, L., Sun, Y., Vlachou, A., Moschos, V., Salazar, G., Szidat, S., Prévôt, A.S.H., Harrison, R.M., Shi, Z., 2021. Source apportionment of carbonaceous aerosols in Beijing with radiocarbon and

- organic tracers: insight into the differences between urban and rural sites. *Atmos. Chem. Phys.* 21 (10), 8273–8292. <https://doi.org/10.5194/acp-21-8273-2021>.
- Huang, K., Fu, J.S., Lin, N.H., Wang, S.H., Dong, X., Wang, G., 2019. Superposition of Gobi Dust and Southeast Asian biomass burning: the effect of multisource long-range transport on aerosol optical properties and regional meteorology modification. *J. Geophys. Res.: Atmospheres* 124 (16), 9464–9483. <https://doi.org/10.1029/2018JD030241>.
- Iinuma, Y., Brüggemann, E., Gnauk, T., Müller, K., Andreae, M.O., Helas, G., Parmar, R., Herrmann, H., 2007. Source characterization of biomass burning particles: the combustion of selected European conifers, African hardwood, savanna grass, and German and Indonesian peat. *J. Geophys. Res. Atmospheres* 112 (8). <https://doi.org/10.1029/2006JD007120>.
- Jian, Y., Fu, T.M., 2014. Injection heights of springtime biomass-burning plumes over peninsular Southeast Asia and their impacts on long-range pollutant transport. *Atmos. Chem. Phys.* 14 (8), 3977–3989. <https://doi.org/10.5194/acp-14-3977-2014>.
- Kawamura, K., Izawa, Y., Mochida, M., Shiraiwa, T., 2012. Ice core records of biomass burning tracers (levoglucosan and dehydroabietic, vanillic and p-hydroxybenzoic acids) and total organic carbon for past 300years in the Kamchatka Peninsula, Northeast Asia. *Geochim. Cosmochim. Acta* 99, 317–329. <https://doi.org/10.1016/j.gca.2012.08.006>.
- Kawichai, S., Prapamontol, T., Chantara, S., Kanyanee, T., 2020. Seasonal Variation and Sources Estimation of PM2.5-Bound PAHs from the ambient air of Chiang Mai City: An All-year-round Study in 2017. 47(5), 958–972.
- Keene, W.C., Pszenny, A. P., Galloway, N., Hawley, M.E., 1986. Sea-Salt Corrections and Interpretation of Constituent Ratios in Marine Precipitation at the University. 91, 6647–6658.
- Kopplitz, S.N., Jacob, D.J., Sulprizio, M.P., Myllyvirta, L., Reid, C., 2017. Burden of disease from rising coal-fired power plant emissions in Southeast Asia. *Environ. Sci. Technol.* 51 (3), 1467–1476. <https://doi.org/10.1021/acs.est.6b03731>.
- Lakey, P.S.J., Berkemeier, T., Tong, H., Arango, A.M., Lucas, K., Pöschl, U., Shiraiwa, M., 2016. Chemical exposure-response relationship between air pollutants and reactive oxygen species in the human respiratory tract. *Sci. Rep.* 6 <https://doi.org/10.1038/srep32916>.
- Lee, C.T., Chuang, M.T., Lin, N.H., Wang, J.L., Sheu, G.R., Chang, S.C., Wang, S.H., Huang, H., Chen, H.W., Liu, Y.L., Weng, G.H., Lai, H.Y., Hsu, S.P., 2011. The enhancement of PM2.5 mass and water-soluble ions of biomass transported from Southeast Asia over the Mountain Lulin site in Taiwan. *Atmos. Environ.* 45 (32), 5784–5794. <https://doi.org/10.1016/j.atmosenv.2011.07.020>.
- Li, Y., Fu, T.M., Yu, J.Z., Feng, X., Zhang, L., Chen, J., Boreddy, S.K.R., Kawamura, K., Fu, P., Yang, X., Zhu, L., Zeng, Z., 2021. Impacts of chemical degradation on the global budget of atmospheric levoglucosan and its use as a biomass burning tracer. *Environ. Sci. Technol.* 55 (8), 5525–5536. <https://doi.org/10.1021/acs.est.0c07313>.
- Li, J., Pósfai, M., Hobbs, P.V., Buseck, P.R., 2003. Individual aerosol particles from biomass burning in southern Africa: 2. Compositions and aging of inorganic particles. *J. Geophys. Res.: Atmospheres* 108 (13), 1–12. <https://doi.org/10.1029/2002jd002310>.
- Liang, Y., Che, H., Gui, K., Zheng, Y., Yang, X., Li, X., Liu, C., Sheng, Z., Sun, T., Zhang, X., 2019. Impact of biomass burning in south and southeast asia on background aerosol in Southwest China. *Aerosol Air Qual. Res.* 19 (5), 1188–1204. <https://doi.org/10.4209/aaqr.2018.08.0324>.
- Lin, P., Hu, M., Deng, Z., Slanina, J., Han, S., Kondo, Y., Takegawa, N., Miyazaki, Y., Zhao, Y., Sugimoto, N., 2009. Seasonal and diurnal variations of organic carbon in PM2.5 in Beijing and the estimation of secondary organic carbon. *J. Geophys. Res. Atmospheres* 114 (11), 1–14. <https://doi.org/10.1029/2008JD010902>.
- Liu, D., Li, J., Zhang, Y., Xu, Y., Liu, X., Ding, P., Shen, C., Chen, Y., Tian, C., Zhang, G., 2013. The use of levoglucosan and radiocarbon for source apportionment of PM 2.5 carbonaceous aerosols at a background site in East China. *Environ. Sci. Technol.* 47 (18), 10454–10461. <https://doi.org/10.1021/es401250k>.
- Liu, J., Li, J., Liu, D., Ding, P., Shen, C., Mo, Y., Wang, X., Luo, C., Cheng, Z., Szidat, S., Zhang, Y., Chen, Y., Zhang, G., 2016. Source apportionment and dynamic changes of carbonaceous aerosols during the haze bloom-decay process in China based on radiocarbon and organic molecular tracers. *Atmos. Chem. Phys.* 16 (5), 2985–2996. <https://doi.org/10.5194/acp-16-2985-2016>.
- Liu, D., Vonwiller, M., Li, J., Liu, J., Szidat, S., Zhang, Y., Tian, C., Chen, Y., Cheng, Z., Zhang, G., Fu, P., Zhang, G., 2020. Fossil and non-fossil fuel sources of organic and elemental carbonaceous aerosol in Beijing, Shanghai, and Guangzhou: Seasonal carbon source variation. *Aerosol Air Qual. Res.* 20 (11), 2495–2506. <https://doi.org/10.4209/aaqr.2019.12.0642>.
- Liu, X., Zhang, Y.L., Peng, Y., Xu, L., Zhu, C., Cao, F., Zhai, X., Mozammel Haque, M., Yang, C., Chang, Y., Huang, T., Xu, Z., Bao, M., Zhang, W., Fan, M., Lee, X., 2019. Chemical and optical properties of carbonaceous aerosols in Nanjing, eastern China: regionally transported biomass burning contribution. *Atmos. Chem. Phys.* 19 (17), 11213–11233. <https://doi.org/10.5194/acp-19-11213-2019>.
- Marlier, M.E., Defries, R.S., Voulgarakis, A., Kinney, P.L., Randerson, J.T., Shindell, D.T., Chen, Y., Faluvegi, G., 2013. El Niño and health risks from landscape fire emissions in southeast Asia. *Nat. Clim. Change* 3 (2), 131–136. <https://doi.org/10.1038/nclimate1658>.
- Mayol-Bracero, O.L., Guyon, P., Graham, B., Roberts, G., Andreae, M.O., Decesari, S., Facchini, M. C., Fuzzi, S., Artaxo, P., 2002. Water-soluble organic compounds in biomass burning aerosols over Amazonia Apportionment of the chemical composition and importance of the polyacidic fraction. *J. Geophys. Res. Atmospheres*, 107(20), LBA 59-1-LBA 59-15. <https://doi.org/10.1029/2001JD000522>.
- Mohn, J., Szidat, S., Fellner, J., Rechberger, H., Quartier, R., Buchmann, B., Emmenegger, L., 2008. Determination of biogenic and fossil CO₂ emitted by waste incineration based on 14CO₂ and mass balances. *Bioresour. Technol.* 99 (14), 6471–6479. <https://doi.org/10.1016/j.biortech.2007.11.042>.
- Myyhre, G., Samset, B.H., Schulz, M., Balkanski, Y., Bauer, S., Bernsten, T.K., Bian, H., Bellouin, N., Chin, M., Diehl, T., Easter, R.C., Feichter, J., Ghan, S.J., Hauglustaine, D., Iversen, T., Kinne, S., Kirkevåg, A., Lamarque, J.-F., Lin, G., Liu, X., Lund, M.T., Luo, G., Ma, X., van Noije, T., Penner, J.E., Rasch, P.J., Ruiz, A., Seland, Ø., Skeie, R.B., Stier, P., Takemura, T., Tsigaridis, K., Wang, P., Wang, Z., Xu, L., Yu, H., Yu, F., Yoon, J.-H., Zhang, K., Zhang, H., Zhou, C., 2013. Radiative forcing of the direct aerosol effect from AeroCom Phase II simulations. *Atmos. Chem. Phys.* 13 (4), 1853–1877.
- Ni, H., Huang, R.J., Cao, J., Liu, W., Zhang, T., Wang, M., Meijer, H.A.J., Dusek, U., 2018. Source apportionment of carbonaceous aerosols in Xi'an, China: insights from a full year of measurements of radiocarbon and the stable isotope 13C. *Atmos. Chem. Phys.* 18 (22), 16363–16383. <https://doi.org/10.5194/acp-18-16363-2018>.
- Palm, B.B., Peng, Q., Fredrickson, C.D., Lee, B.H., Garofalo, L.A., Pothier, M.A., Kreidenweis, S.M., Farmer, D.K., Korkhrel, R.P., Shen, Y., Murphy, S.M., Permar, W., Hu, L., Campos, T.L., Hall, S.R., Ullmann, K., Zhang, X., Flocke, F., Fischer, E.V., Thornton, J.A., 2020. Quantification of organic aerosol and brown carbon evolution in fresh wildfire plumes. *PNAS* 117 (47), 29469–29477. <https://doi.org/10.1073/pnas.2012218117>.
- Pani, S.K., Lin, N.H., Chantara, S., Wang, S.H., Khamkaew, C., Prapamontol, T., Janjai, S., 2018. Radiative response of biomass-burning aerosols over an urban atmosphere in northern peninsular Southeast Asia. *Sci. Total Environ.* 633, 892–911. <https://doi.org/10.1016/j.scitotenv.2018.03.204>.
- Peltier, R.E., Hecobian, A.H., Weber, R.J., Stohl, A., Atlas, E.L., Riemer, D.D., Blake, D.R., Apel, E., Campos, T., Karl, T., 2008. Investigating the sources and atmospheric processing of fine particles from Asia and the Northwestern United States measured during INTEX B. *Atmos. Chem. Phys.* 8 (6), 1835–1853. <https://doi.org/10.5194/acp-8-1835-2008>.
- Phairuang, W., Suwattiga, P., Chetiyankornkul, T., Hongtieab, S., Limpaseni, W., Ikemori, F., Hata, M., Furuuchi, M., 2019. The influence of the open burning of agricultural biomass and forest fires in Thailand on the carbonaceous components in size-fractionated particles. *Environ. Pollut.* 247, 238–247. <https://doi.org/10.1016/j.envpol.2019.01.001>.
- Platt, S.M., Haddad, I.E., Pieber, S.M., Huang, R.-J., Zardini, A.A., Clairrotte, M., Suarez-Bertoa, R., Barmet, P., Pfaffenberger, L., Wolf, R., Slowik, J.G., Fuller, S.J., Kalberer, M., Chirico, R., Dommen, J., Astorga, C., Zimmermann, R., Marchand, N., Hellebust, S., Temime-Roussel, B., Baltensperger, U., Prévôt, A.S.H., 2014. Two-stroke scooters are a dominant source of air pollution in many cities. *Nat. Commun.* 5 (1) <https://doi.org/10.1038/ncomms4749>.
- Pongpiachan, S., Hattayanone, M., Cao, J., 2017. Effect of agricultural waste burning season on PM 2.5-bound polycyclic aromatic hydrocarbon (PAH) levels in Northern Thailand.
- Rauber M., Salazar G., Yttri K. Y., Szidat S. (Unpublished results). An Optimised OC/EC Fraction Separation Method for Radiocarbon Source Apportionment Applied to Low-Loaded Arctic Aerosol Filters.
- Rauber, M., Salazar, G., 2022. martin-rauber/compycal: (v1.2.2). Zenodo. <https://doi.org/10.5281/zenodo.5958275>.
- Reddington, C.L., Butt, E.W., Ridley, D.A., Artaxo, P., Morgan, W.T., Coe, H., Spracklen, D.V., 2015. Air quality and human health improvements from reductions in deforestation-related fire in Brazil. *Nat. Geosci.* 8 (10), 768–771. <https://doi.org/10.1038/ngeo2535>.
- Reimer, P.-J., Brown, T.A., Reimer, R.W., 2004. Discussion: Reporting and calibration of post-bomb 14C data. *Radiocarbon* 46 (3), 1299–1304. <https://doi.org/10.1017/S0033822200033154>.
- Saarikoski, S., Timonen, H., Saarnio, K., Aurela, M., Järvi, L., Keronen, P., Kerminen, V.-M., Hillamo, R., 2008. Sources of organic carbon in fine particulate matter in northern European urban air. *Atmos. Chem. Phys.* 8 (20), 6281–6295.
- Salma, I., Németh, Z., Weidinger, T., Maenhaut, W., Claeys, M., Molnár, M., Major, I., Ajtai, T., Utry, N., Bozók, Z., 2017. Source apportionment of carbonaceous chemical species to fossil fuel combustion, biomass burning and biogenic emissions by a coupled radiocarbon-levoglucosan marker method. *Atmos. Chem. Phys.* 17 (22), 13767–13781. <https://doi.org/10.5194/acp-17-13767-2017>.
- Schmidl, C., Marr, I.L., Caseiro, A., Kotianová, P., Berner, A., Bauer, H., Kasper-Giebl, A., Puxbaum, H., 2008. Chemical characterisation of fine particle emissions from wood stove combustion of common woods growing in mid-European Alpine regions. *Atmos. Environ.* 42 (1), 126–141. <https://doi.org/10.1016/j.atmosenv.2007.09.028>.
- Sheesley, R.J., Schauer, J.J., Chowdhury, Z., Cass, G.R., Simoneit, B.R.T., 2003. Characterization of organic aerosols emitted from the combustion of biomass indigenous to South Asia. *J. Geophys. Res.: Atmospheres* 108 (D9), n/a–n/a.
- Sheu, G.R., Lin, N.H., Wang, J.L., Lee, C.T., Ou Yang, C.F., Wang, S.H., 2010. Temporal distribution and potential sources of atmospheric mercury measured at a high-elevation background station in Taiwan. *Atmos. Environ.* 44 (20), 2393–2400. <https://doi.org/10.1016/j.atmosenv.2010.04.009>.
- Simoneit, B.R.T., Schauer, J.J., Nolte, C.G., Oros, D.R., Elias, V.O., Fraser, M.P., Rogge, W.F., Cass, G.R., 1999. <Simoneit levoglucosan.pdf>. *Atmos. Environ.* 33 (2), 1–10 [https://doi.org/10.1016/S0950-0687\(99\)00073-4](https://doi.org/10.1016/S0950-0687(99)00073-4).
- Suciu, L.G., Masiello, C.A., Griffin, R.J., 2019. Anhydrosugars as tracers in the Earth system. *Biogeochemistry* 146 (3), 209–256.
- Sun, J., Shen, Z., Zhang, Y., Zhang, Q., Lei, Y., Huang, Y., Niu, X., Xu, H., Cao, J., Ho, S.H., Li, X., 2019. Characterization of PM2.5 source profiles from typical biomass burning of maize straw, wheat straw, wood branch, and their processed products (briquette and charcoal) in China. *Atmos. Environ.* 205, 36–45.
- Szidat, S., Jenk, T.M., Gäggeler, H.W., Synal, H.A., Fisseha, R., Baltensperger, U., Kalberer, M., Samburova, V., Wacker, L., Saurer, M., Schwikowski, M., Hajdas, I., 2004. Source apportionment of aerosols by 14C measurements in different

- carbonaceous particle fractions. *Radiocarbon* 46 (1), 475–484. <https://doi.org/10.1017/S003822200039783>.
- Szidat, S., Salazar, G.A., Vogel, E., Battaglia, M., Wacker, L., Ssynal, H.-A., Türler, A., 2014. 14 C Analysis and sample preparation at the new bern laboratory for the Analysis of Radiocarbon with AMS (LARA). *Radiocarbon* 56 (2), 561–566. <https://doi.org/10.2458/56.17457>.
- Tet, S., Muttamara, S., Laortanakul, P., 2002. Influence of benzene emission from motorcycles on Bangkok air quality 36, 651–661.
- Tsai, Y.L., Sopajaree, K., Chotruksa, A., Wu, H.C., Kuo, S.C., 2013. Source indicators of biomass burning associated with inorganic salts and carboxylates in dry season ambient aerosol in Chiang Mai Basin, Thailand. *Atmos. Environ.* 78, 93–104. <https://doi.org/10.1016/j.atmosenv.2012.09.040>.
- Tsay, S.-C., Hsu, N.C., Lau, W.-M., Li, C., Gabriel, P.M., Ji, Q., Holben, B.N., Judd Welton, E., Nguyen, A.X., Janjai, S., Lin, N.-H., Reid, J.S., Boonjawat, J., Howell, S. G., Huebert, B.J., Fu, J.S., Hansell, R.A., Sayer, A.M., Gautam, R., Wang, S.-H., Goodloe, C.S., Mikko, L.R., Shu, P.K., Loftus, A.M., Huang, J., Kim, J.Y., Jeong, M.-J., Pantina, P., 2013. From BASE-ASIA toward 7-SEAS: a satellite-surface perspective of boreal spring biomass-burning aerosols and clouds in Southeast Asia. *Atmos. Environ.* 78, 20–34.
- Vlachou, A., Daellenbach, K.R., Bozzetti, C., Chazeanu, B., Salazar, G.A., Szidat, S., Jaffrezo, J.L., Hueglin, C., Baltensperger, U., El Haddad, I., Prévôt, A.S.H., 2018. Advanced source apportionment of carbonaceous aerosols by coupling offline AMS and radiocarbon size-segregated measurements over a nearly 2-year period. *Atmos. Chem. Phys.* 18 (9), 6187–6206. <https://doi.org/10.5194/acp-18-6187-2018>.
- Weber, R.J., Sullivan, A.P., Peltier, R.E., Russell, A., Yan, B., Zheng, M., de Grouw, J., Warneke, C., Brock, C., Holloway, J.S., Atlas, E.L., Edgerton, E., 2007. A study of secondary organic aerosol formation in the anthropogenic-influenced southeastern United States. *J. Geophys. Res. Atmospheres* 112 (13), 1–13. <https://doi.org/10.1029/2007JD008408>.
- Wozniak, A.S., Bauer, J.E., Dickhut, R.M., 2012a. Characteristics of water-soluble organic carbon associated with aerosol particles in the eastern United States. *Atmos. Environ.* 46, 181–188. <https://doi.org/10.1016/j.atmosenv.2011.10.001>.
- Wozniak, A.S., Bauer, J.E., Dickhut, R.M., Xu, L., McNichol, A.P., 2012b. Isotopic characterization of aerosol organic carbon components over the eastern United States. *J. Geophys. Res. Atmospheres* 117 (13), 1–14. <https://doi.org/10.1029/2011JD017153>.
- Wu, X., Cao, F., Haque, M.M., Fan, M.Y., Zhang, S.C., Zhang, Y.L., 2020. Molecular composition and source apportionment of fine organic aerosols in Northeast China. *Atmos. Environ.* 239 (June), 117722 <https://doi.org/10.1016/j.atmosenv.2020.117722>.
- Yin, S., Wang, X., Zhang, X., Guo, M., Miura, M., Xiao, Y., 2019. Influence of biomass burning on local air pollution in mainland Southeast Asia from 2001 to 2016. *Environ. Pollut.* 254, 112949 <https://doi.org/10.1016/j.envpol.2019.07.117>.
- Yoon, S., Fairley, D., Barrett, T.E., Sheesley, R.J., 2018. Biomass and fossil fuel combustion contributions to elemental carbon across the San Francisco Bay Area. *Atmos. Environ.* 195, 229–242. <https://doi.org/10.1016/j.atmosenv.2018.09.050>.
- Yttri, K.E., Simpson, D., Stenstrom, K., Puxbaum, H., Svendby, T., 2011. Source apportionment of the carbonaceous aerosol in Norway & quantitative estimates based on 14C, thermal-optical and organic tracer analysis. *Atmos. Chem. Phys.* 11 (17), 9375–9394. <https://doi.org/10.5194/acp-11-9375-2011>.
- Zhang, Y.L., Perron, N., Ciobanu, V.G., Zotter, P., Mingüillón, M.C., Wacker, L., Prévôt, A.S.H., Baltensperger, U., Szidat, S., 2012. On the isolation of OC and EC and the optimal strategy of radiocarbon-based source apportionment of carbonaceous aerosols. *Atmos. Chem. Phys.* 12 (22), 10841–10856.
- Zhang, Y.L., Zotter, P., Perron, N., Prévôt, A.S.H., Wacker, L., Szidat, S., 2013. Fractions in Fine and Coarse Particles By Radiocarbon Measurement. *Radiocarbon* 55 (2), 1510–1520.
- Zhang, Y.L., Li, J., Zhang, G., Zotter, P., Huang, R.J., Tang, J.H., Wacker, L., Prévôt, A.S.H., Szidat, S., 2014. Radiocarbon-based source apportionment of carbonaceous aerosols at a regional background site on Hainan Island, South China. *Environ. Sci. Technol.* 48 (5), 2651–2659. <https://doi.org/10.1021/es4050852>.
- Zhang, Y.L., Huang, R.J., El Haddad, I., Ho, K.F., Cao, J.J., Han, Y., Zotter, P., Bozzetti, C., Daellenbach, K.R., Canonaco, F., Slowik, J.G., Salazar, G., Schwikowski, M., Schnelle-Kreis, J., Abbaszade, G., Zimmermann, R., Baltensperger, U., Prévôt, A.S.H., Szidat, S., 2015a. Fossil vs. non-fossil sources of fine carbonaceous aerosols in four Chinese cities during the extreme winter haze episode of 2013. *Atmos. Chem. Phys.* 15 (3), 1299–1312. <https://doi.org/10.5194/acp-15-1299-2015>.
- Zhang, Y., Ren, H., Sun, Y., Cao, F., Chang, Y., Liu, S., Lee, X., Agrios, K., Kawamura, K., Liu, D., Ren, L., Du, W., Wang, Z., Prévôt, A.S.H., Szidat, S., Fu, P., 2017. High contribution of nonfossil sources to submicrometer organic aerosols in Beijing, China. *Environ. Sci. Technol.* 51 (14), 7842–7852. <https://doi.org/10.1021/acs.est.7b01517>.
- Zhang, Y.L., Schnelle-Kreis, J., Abbaszade, G., Zimmermann, R., Zotter, P., Shen, R.R., Schäfer, K., Shao, L., Prévôt, A.S.H., Szidat, S., 2015b. Source apportionment of elemental carbon in Beijing, China: insights from radiocarbon and organic marker measurements. *Environ. Sci. Technol.* 49 (14), 8408–8415. <https://doi.org/10.1021/acs.est.5b01944>.
- Zhang, Y.-X., Shao, M., Zhang, Y.-H., Zeng, L.-M., He, L.-Y., Zhu, B., Wei, Y.-J., Zhu, X.-L., 2007. Source profiles of particulate organic matters emitted from cereal straw burnings. *J. Environ. Sci.* 19 (2), 167–175.
- Zheng, L., Yang, X., Lai, S., Ren, H., Yue, S., Zhang, Y., Huang, X., Gao, Y., Sun, Y., Wang, Z., Fu, P., 2018. Impacts of springtime biomass burning in the northern Southeast Asia on marine organic aerosols over the Gulf of Tonkin, China. *Environ. Pollut.* 237, 285–297. <https://doi.org/10.1016/j.envpol.2018.01.089>.